X-951-75-235
PREPRINT

REVIEW OF DATA ANALYSIS PROCEDURES FOR THE ATS-6 MILLIMETER WAVE EXPERIMENT

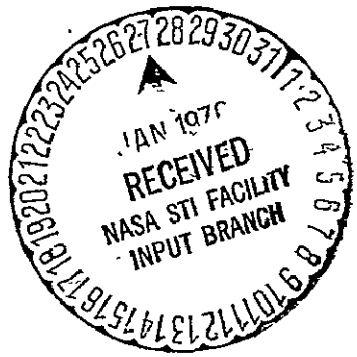

AUGUST 1975

GODDARD SPACE FLIGHT CENTER
GREENBELT, MARYLAND

For information concerning availability
of this document contact:

Technical Information Division, Code 250
Goddard Space Flight Center
Greenbelt, Maryland 20771

(Telephone 301-982-4488)

X-951-75-235

REVIEW OF DATA ANALYSIS PROCEDURES

FOR THE

ATS-6 MILLIMETER WAVE EXPERIMENT

Robert Meneghini

Telecommunications Systems Branch
Communications and Navigation Division
Applications Directorate

August 1975

GODDARD SPACE FLIGHT CENTER
Greenbelt, Maryland

REVIEW OF DATA ANALYSIS PROCEDURES FOR THE ATS-6 MILLIMETER WAVE EXPERIMENT

Robert Meneghini

ABSTRACT

Predictions of satellite downlink attenuation through the use of ground-based measurements form a substantial part of the ATS-6 Millimeter Wave Experiment (MWE). At the downlink frequencies (20 and 30 GHz), the major causes of attenuation are the density and the size distribution of rain drops along the propagation path. Ground station data, which include radar and rain gauge records, measure quantities related to the meteorological parameters of interest and thereby provide a prediction of downlink attenuation with which the measured attenuation can be compared.

The calibration and data analysis procedures used in the MWE are reviewed with the object of improving the accuracy of such ground-based predictions.

It is hoped that some of the suggested changes can be incorporated into the present data analysis procedures. More elaborate data handling and calibration techniques will require further evaluation and interim testing to establish their applicability to the Communications Technology Satellite and planned reuse of the ATS-6 MWE.

CONTENTS

	Page
CALIBRATION TECHNIQUES	1
Introduction	1
Z-R Relations	2
Calibration Procedure	16
FUNCTIONAL RELATION BETWEEN SURFACE AND ELEVATED RAIN RATES	17
Experimental Procedure	17
Theoretical Procedure	22
TWO FREQUENCY RADAR TECHNIQUES	24
Goldhirsh-Katz Method	24
Alternative Technique	35
PHASE DIFFERENCE INFORMATION RELATED TO METEOROLOGICAL PARAMETERS	46
DISCUSSION	53
REFERENCES	61
APPENDIX A – Z-R RELATIONS	63
APPENDIX B – K-Z RELATIONS	65

ILLUSTRATIONS

Figure		Page
1	Storm Cell Structure	4
2	Rain Rates vs Range	5
3	Radar Direction Notation	19
4	Rain Rate vs Time at 884 Meters	25
5	Rain Rate vs Time at 330 Meters	26
6	Radar vs Rainbucket Rain Rate	32
7	Rain Rate vs Drop Size	41
8	Notation for Path Length	47
9	720 MHz Sideband Phase vs Time	54

TABLES

Table		Page
1	Values of Alpha for $\beta = 0.887$	15
2	Comparative Attenuation Results	30
3	Phase Changes for Different Rain Rates	39
4	Rain Rate Values	52

REVIEW OF DATA ANALYSIS PROCEDURES FOR THE ATS-6 MILLIMETER WAVE EXPERIMENT

CALIBRATION TECHNIQUES

Introduction

For the ATS-6 MMW experiment, predictions of the 20 and 30 GHz downlink attenuations are found by measurements of rain rate.* The rain rate, in turn, is related to attenuation by means of scattering theory as applied to independent spherical scatterers along with experimental measurements of rain rate vs drop size distribution.[1,2]

At Rosman, radars at 3.0 and 8.75 GHz, situated near the receiver, are pointed along the downlink path (42° with respect to the horizontal). For each radar, an integrated series of return pulses (1800) provide an estimate of the return power, and thus reflectivity, at locations spaced 100 m apart beginning at a distance 300 m out from the radar. (Note that in this report a specific 100 m cell is sometimes designated a range bin or db Z bin). From the measured reflectivity (Z), the rain rate (R) can be estimated by a number of experimentally or theoretically derived formulas. Details of the radar system can be found in the Westinghouse reports.[3]

Through the use of ten rain gauge buckets situated under the downlink path, the ground rain rate is directly recorded. The data set or its time shifted extrapolated version (if the attempt is made to account for time and spatial differences between height and ground measurements) is then used in the same predictive capacity as that of the radars.

---

* An exception is the measurement of sky temperature which, with an appropriate atmospheric model, provides a direct prediction of expected attenuation. Radiometric measurements, however, are not discussed in this report.

Z-R Relations

A useful measurement for the analysis of radar data is an absolute calibration of the radar. Since radar reflectivity, Z, is used primarily for the determination of rain rate, fixing an empirical relation between these two quantities is essential. The standard relation $Z = 200\ R^{1.6}$ has certain disadvantages:

- The variance between the predicted R and the measured R is large, a result due not only to averages taken over different systems and different locations but also to the inherent variability in the quantity Z being measured.

- The reflectivity factor Z is a function of the back-scattering cross-section, which in turn is a function of frequency—a dependence which becomes more pronounced as the drop sizes increase (i.e. as the deviation from the Rayleigh approximation increases). The Z-R relations change with the radar frequency used. In fact using the data of Medhurst[1], Setzer[2] and Stephen[4], the following expressions (derived in Appendix A) result

$$\begin{aligned} Z_{3.0} &= 315.5\ R^{1.457} \\ Z_{8.75} &= 307.1\ R^{1.546} \end{aligned} \qquad (1)$$

- The actual values of the reflectivity factor of 8.75 GHz are obscured by the effects of signal attenuation. Again using the Medhurst and Setzer data, the difference in attenuation between 8.75 and 3.0 GHz radar (derived in Appendix B) is

$$\begin{aligned} \Delta k\ (\text{db/km}) &\approx 0.006569\ R^{1.29} && \approx k_{tot} \\ \Delta k\ (\text{db/km}) &\approx 3.99 \times 10^{-5}\ Z_{3.0}^{0.88} && \approx k_{tot} \\ \Delta k\ (\text{db/km}) &\approx 5.544 \times 10^{-5}\ Z_{8.75}^{0.83} && \approx k_{tot} \end{aligned} \qquad (2)$$

The reflectivity factor from the 8.75 GHz radar should be greater than that of the 3.0 GHz radar for rain rates greater than about 2 mm/hr. For example, for an R = 50 mm/hr, $dbZ_{8.75} - dbZ_{3.0} \approx 1.4$. This statement, however, holds only if the selective signal attenuation at 8.75 is first taken into account. For example, writing out the radar equations for the 8.75 and 3.0 GHz radars:

$$P_8 = \frac{C_8 Z_8}{r^2} \; e^{-2\int_0^r k\, dr}$$

$$P_3 = \frac{C_3 Z_3}{r^2}$$

Rearranging

$$Z_3 = r^2 P_3 / C_3 \tag{3}$$

and

$$Z'_8 = r^2 P_8 / C_8 = Z_8 e^{-2\int_0^r k\, dr} \tag{4}$$

Z_3 and Z'_8 would be the reflectivity factors computed from the radar return power if all attenuation effects were ignored. Since the attenuation effect is cumulative it becomes more pronounced with an increase in range. At the near range cells (small r) $Z'_8 > Z_3$ as it should be for agreement with rain rate predictions of Equation 1. As range increases, however, $e^{-2\int_0^r k\, dr}$ decreases with a corresponding decrease in Z'_8. For large enough k, $Z'_8 < Z_3$ beginning at some range r_o and continuing thereafter. As a result, Z_3 and Z'_8 will lead to differing predictions of rain rate.

This type of behavior is shown in Figure 1, which plots dbZ vs range.[4] The dbZ'_8 values dominate up to $r \approx 1.5$ km, after which dbZ'_8 drops and remains less than dbZ_3.

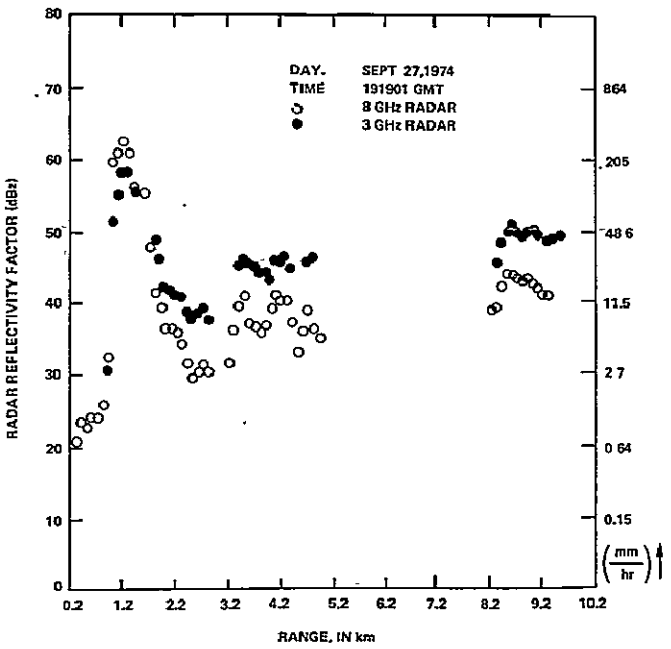

Figure 1. Storm Cell Structure

If attenuation effects of the 8.75 GHz signal are taken into account and different Z-R relations are used (depending on the radar frequency), the rain rates predicted by the two radars exhibit a better agreement than if attenuation effects are neglected and the same Z-R relation is used throughout.

Figure 2 gives the rain rates predicted from four-second averages of the radar data. The plot marked "Standard Prediction" plots $Z = 200 R^{1.6}$ for both radars without attenuation effects. The plot marked "Altered Prediction" uses Equations (1) and (2).

The equations given by Ippolito[6] relate rain rate to downlink attenuation by

$$\alpha_{20}(\text{db}) = \sum_{i=1}^{N} 0.0687\ RR_i^{1.1}\ (0.1) \qquad (5)$$

$$\alpha_{30}(\text{db}) = \sum_{i=1}^{N} 0.1649\ RR^{1.035}\ (0.1)$$

N = number of range bins

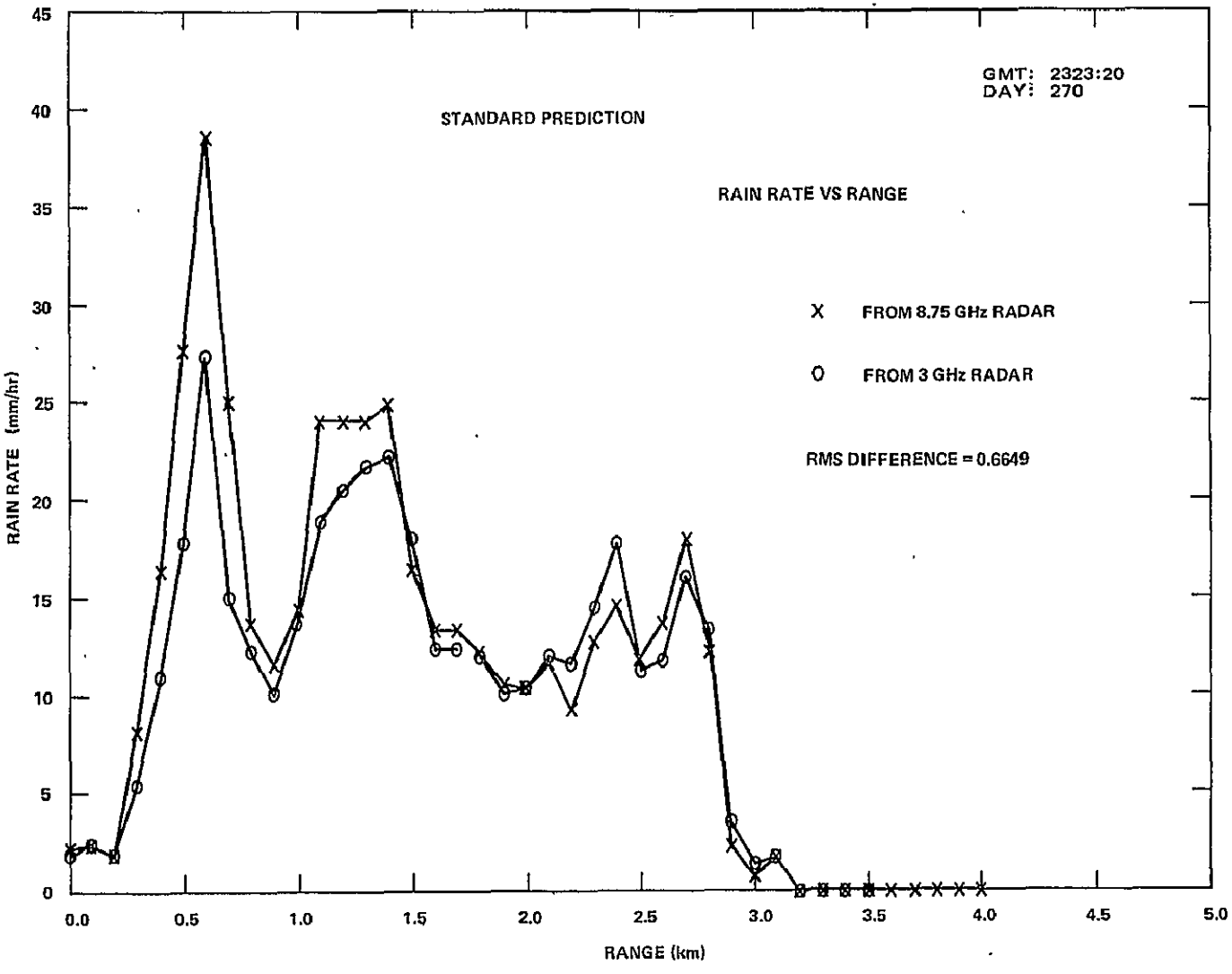

Figure 2. Rain Rates vs Range

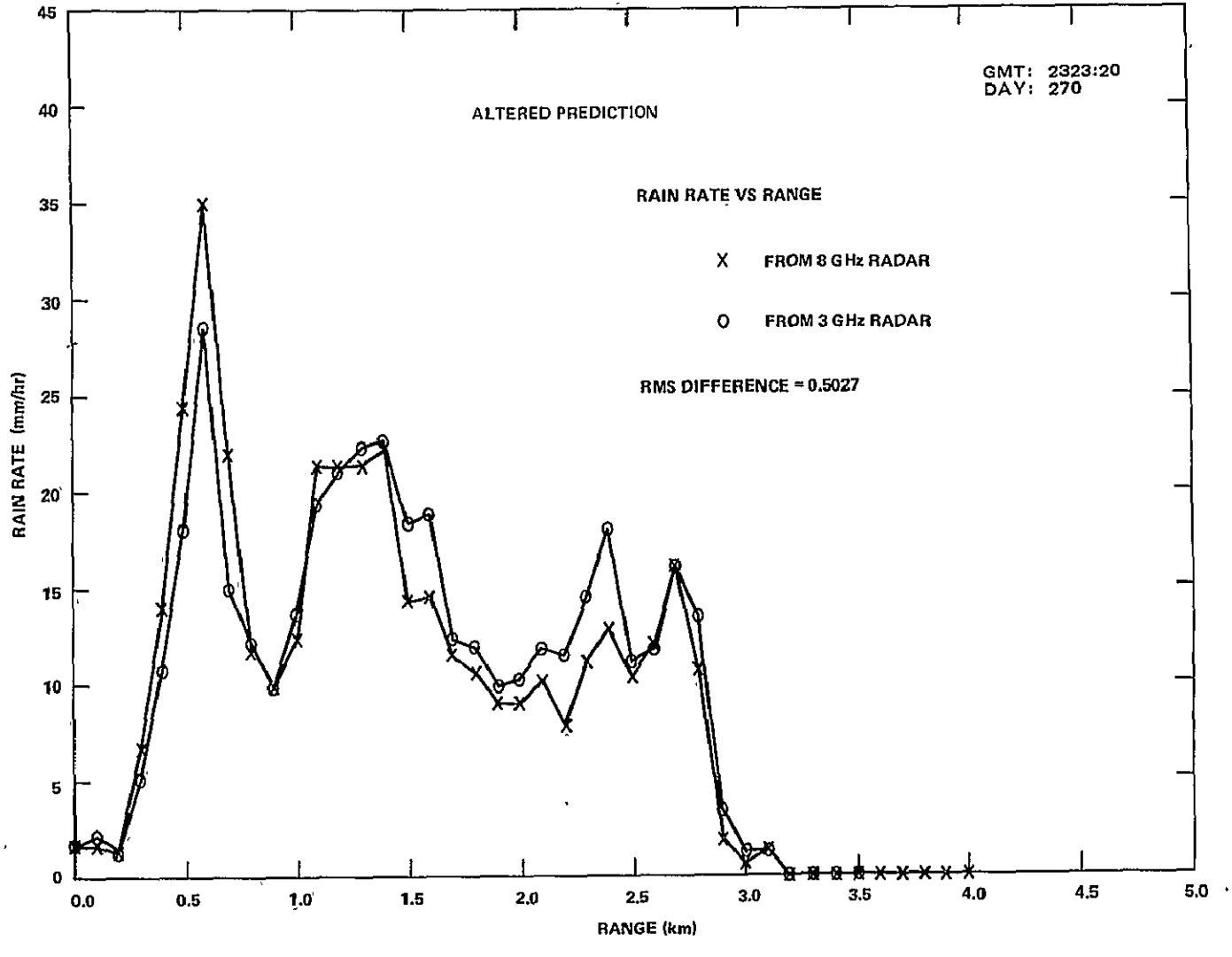

Figure 2. Rain Rates vs Range (Continued)

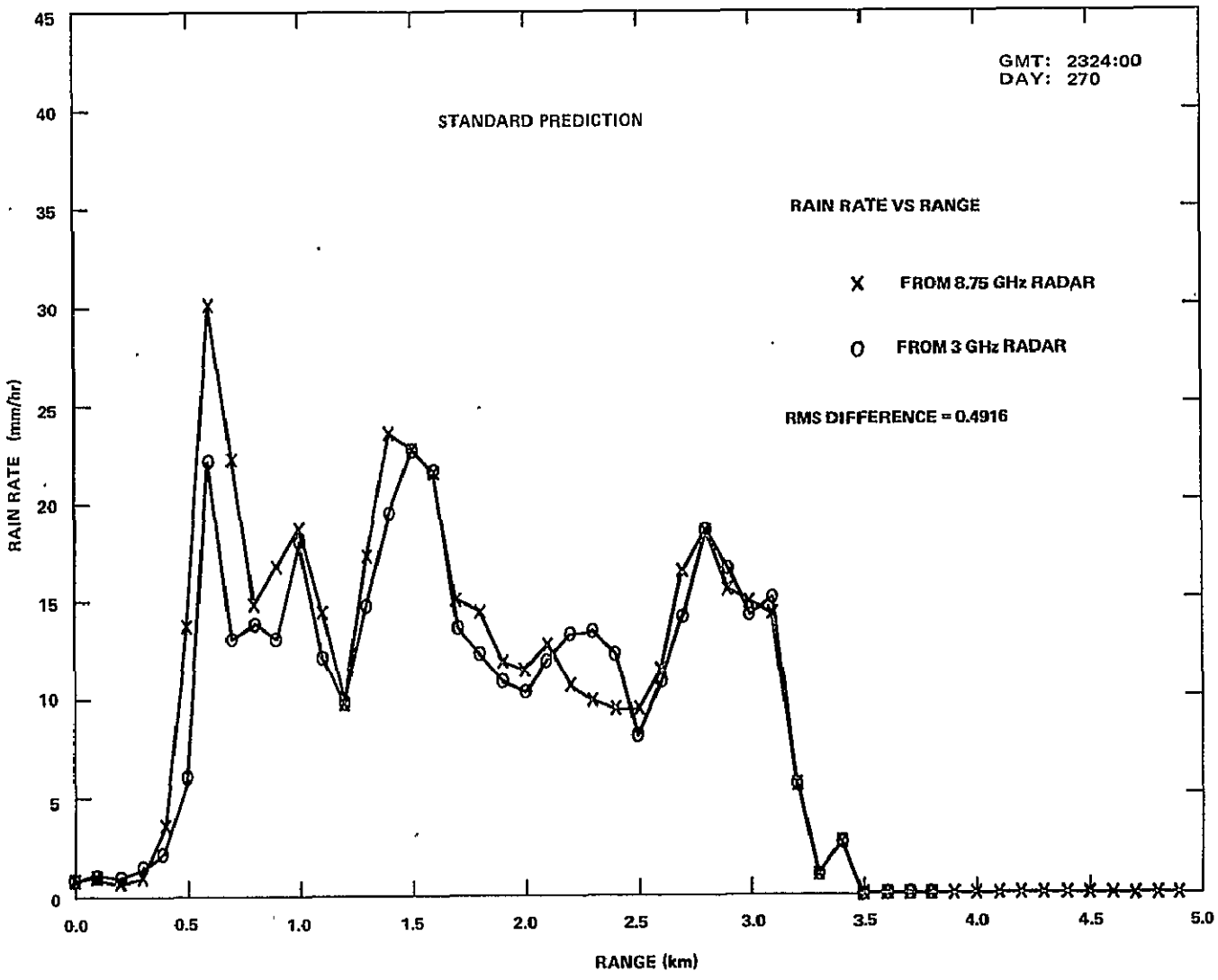

Figure 2. Rain Rate vs Range (Continued)

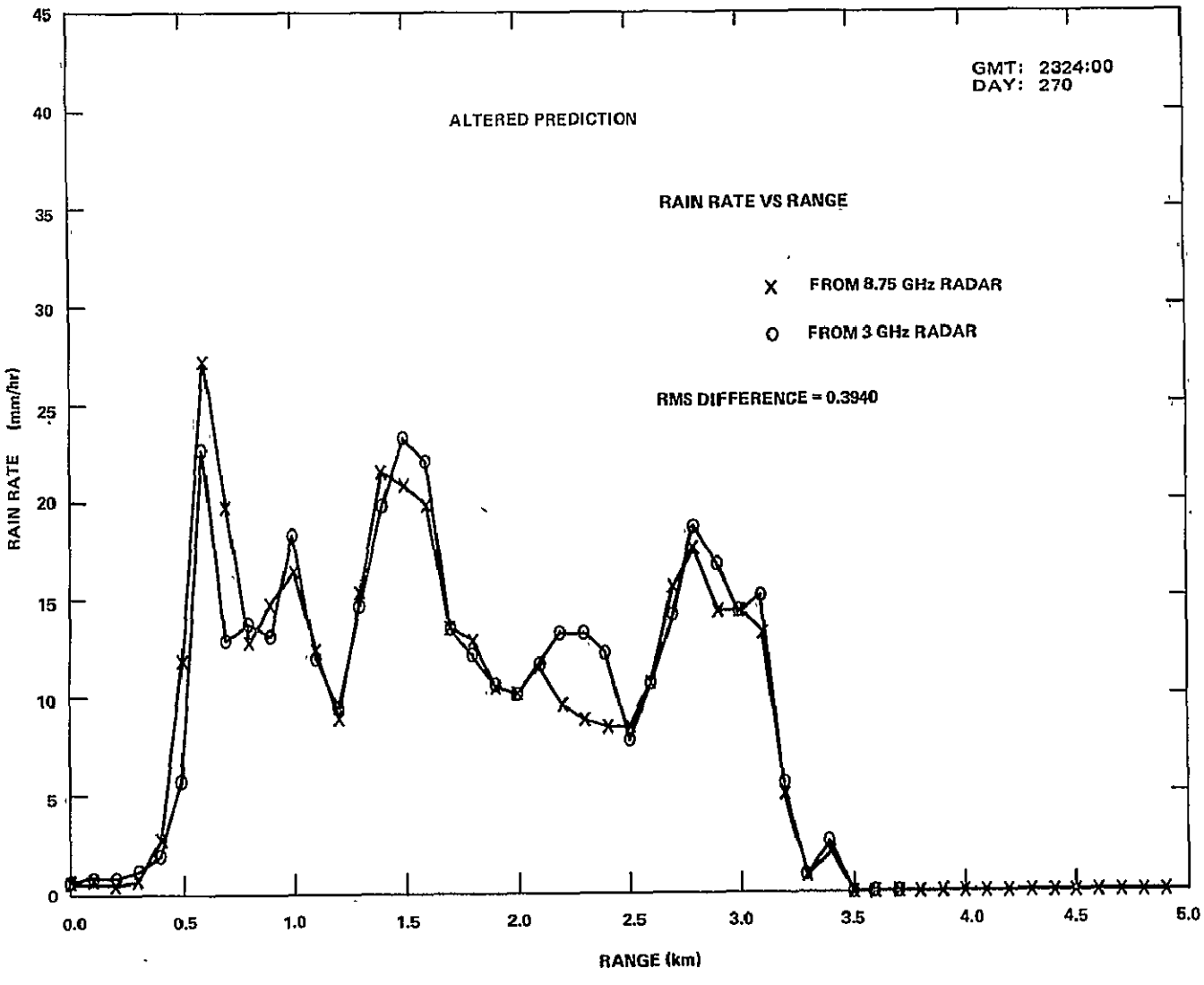

Figure 2. Rain Rates vs Range (Continued)

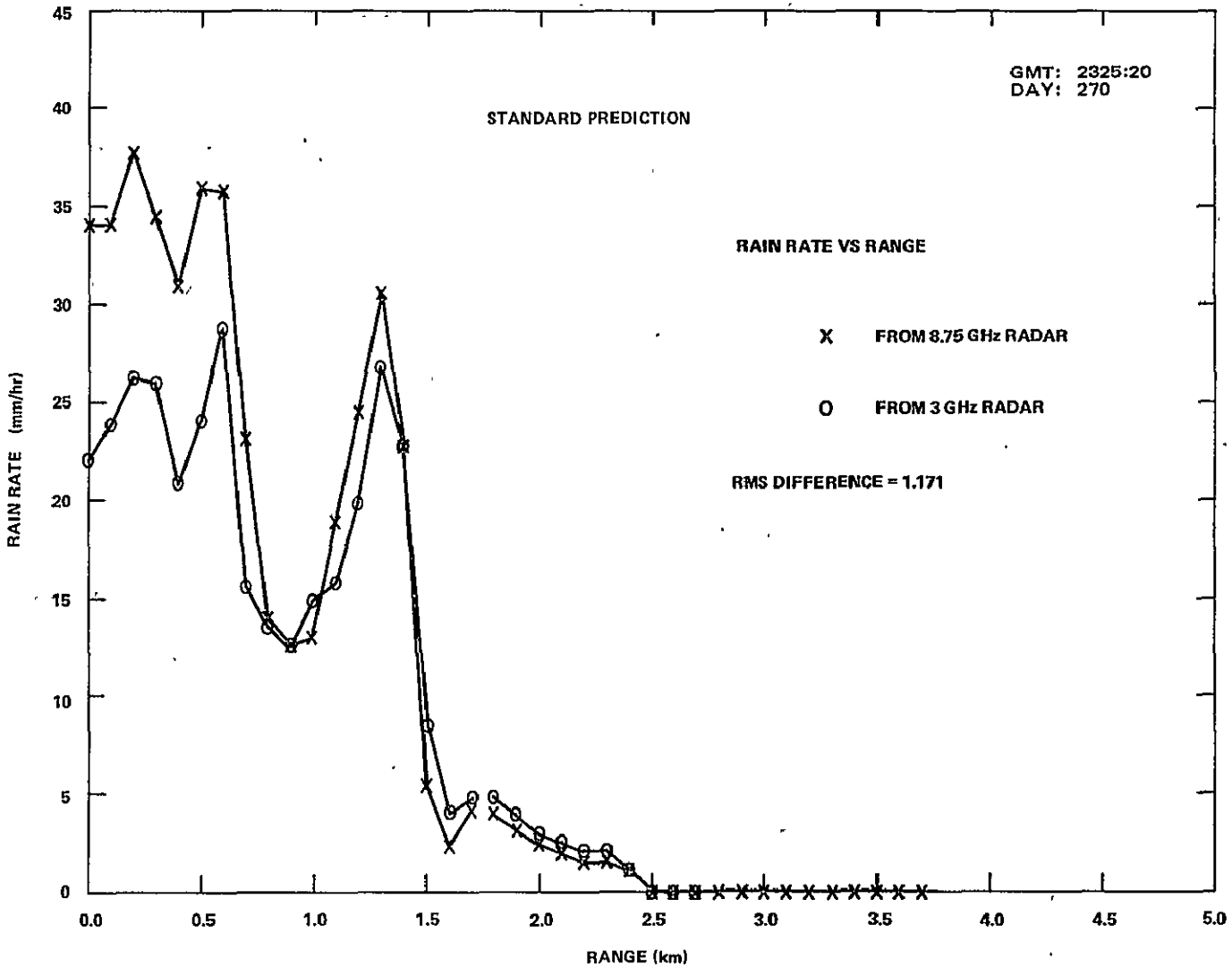

Figure 2. Rain Rates vs Range (Continued)

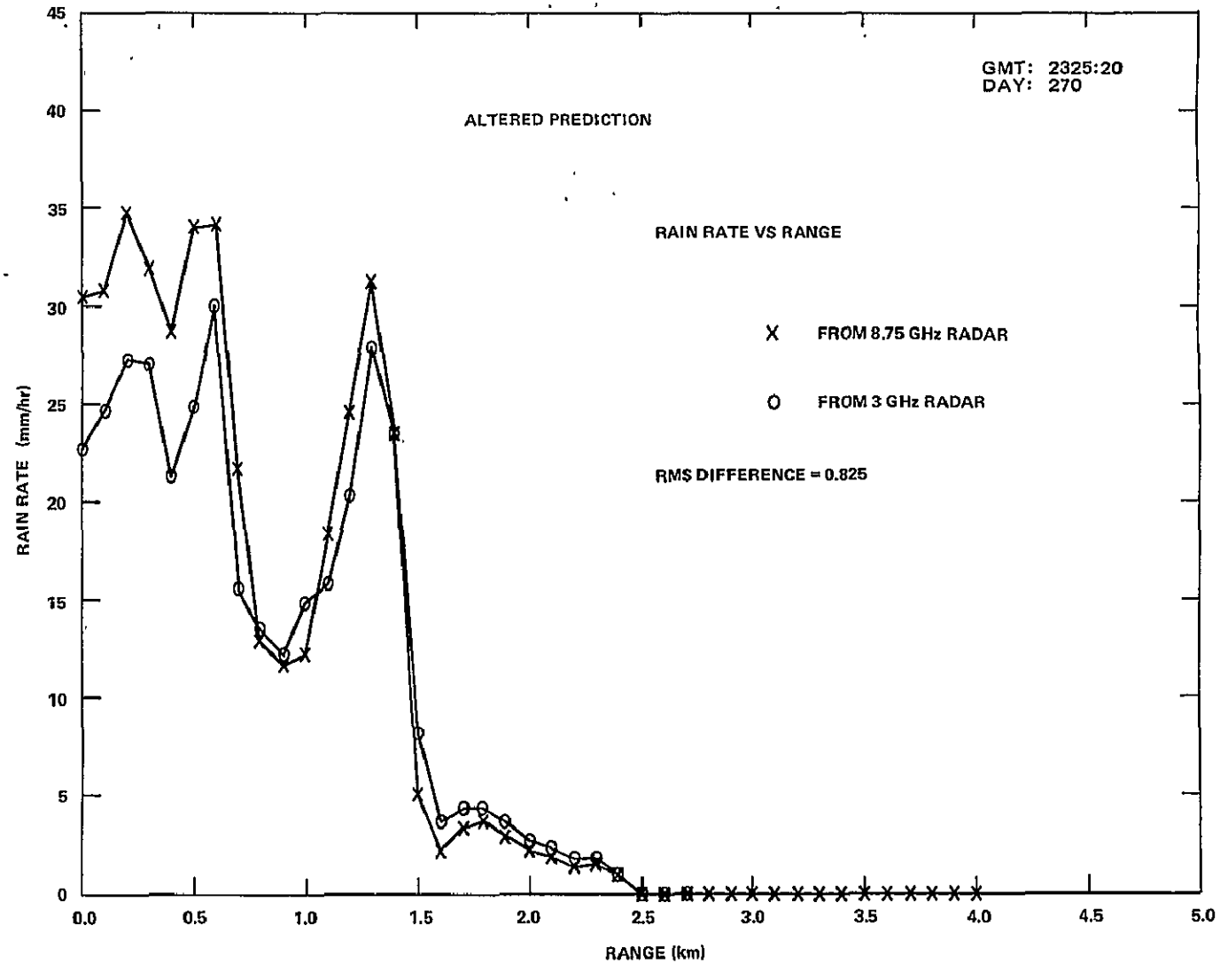

Figure 2. Rain Rates vs Range (Continued)

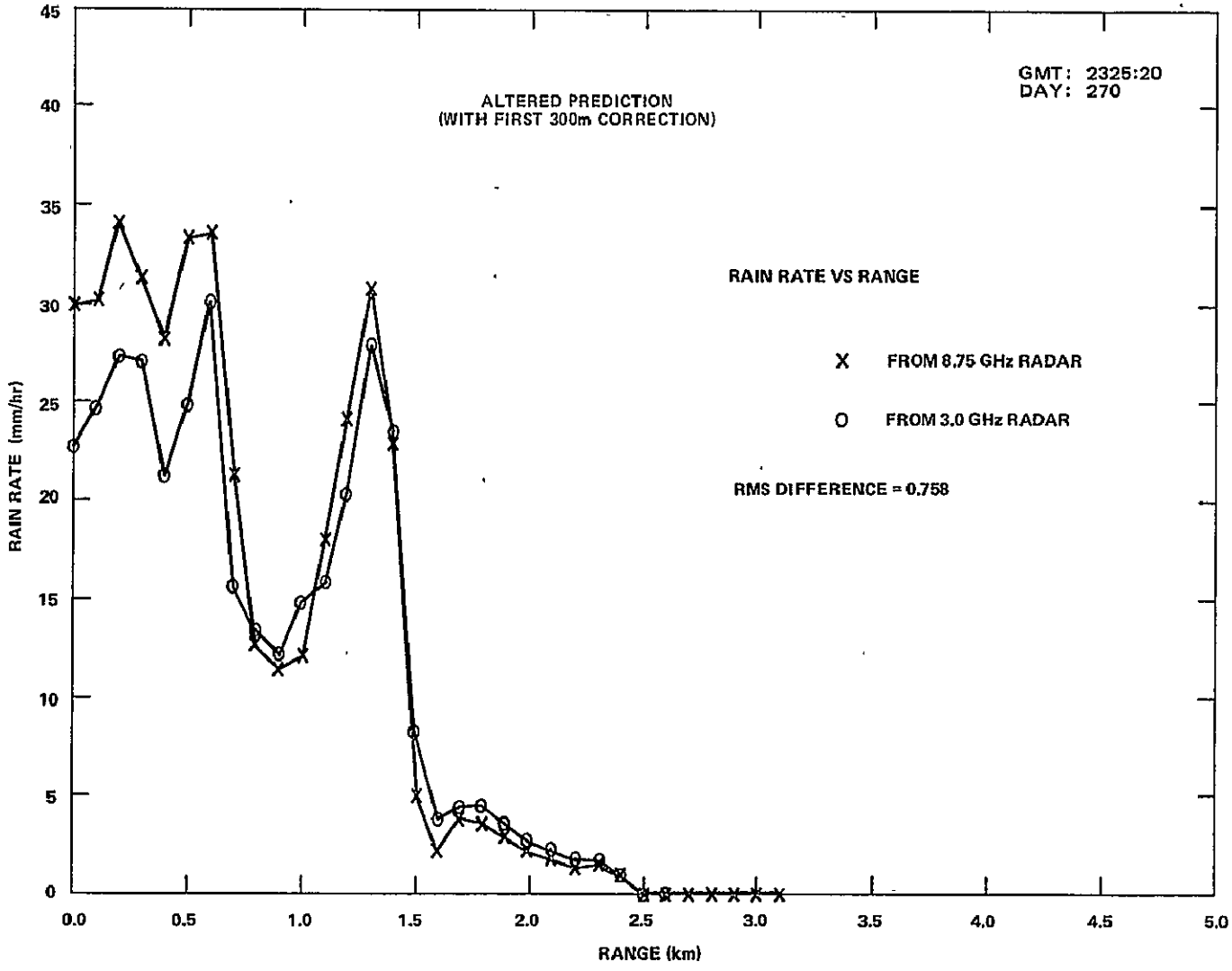

Figure 2. Rain Rates vs Range (Continued)

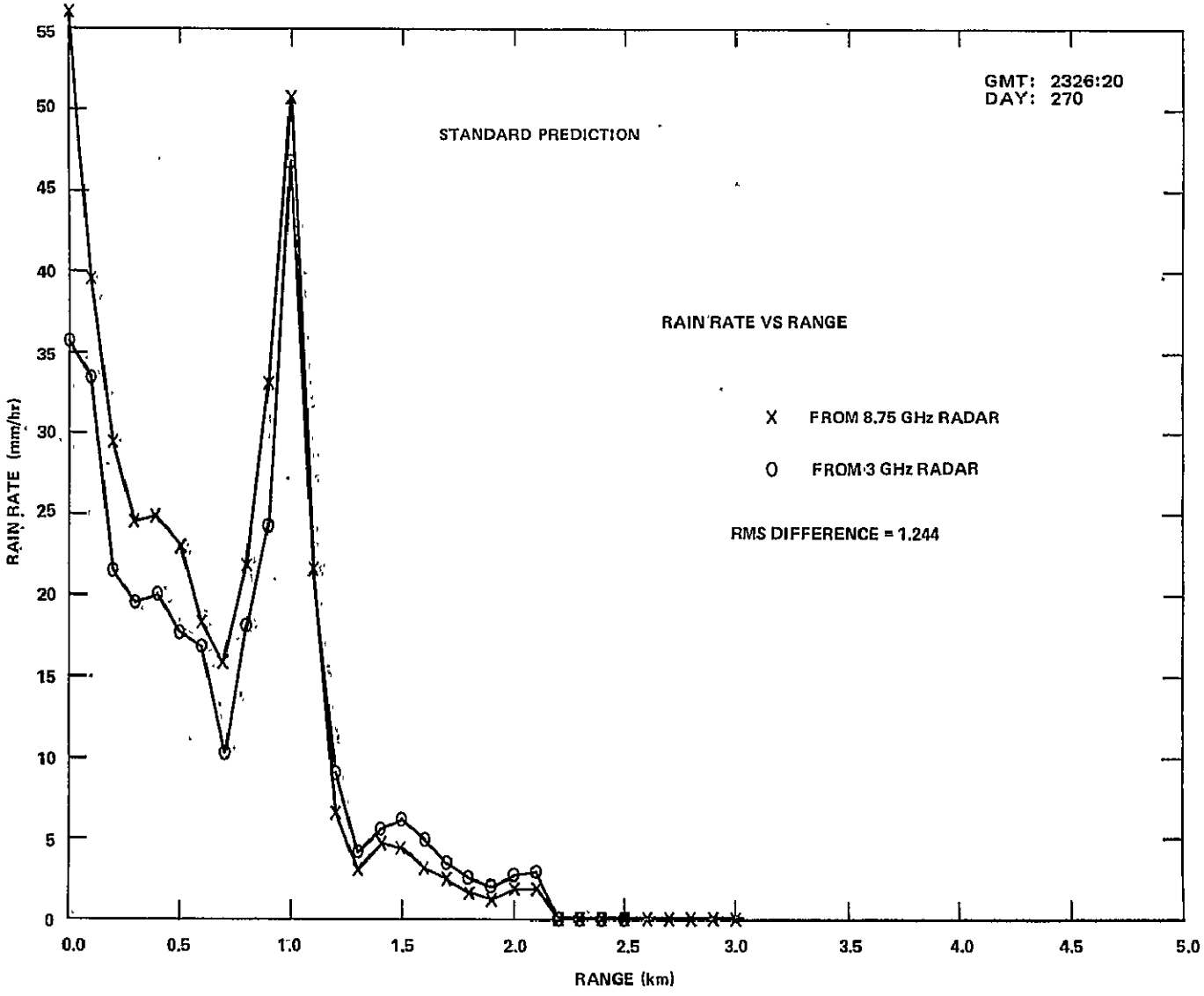

Figure 2. Rain Rates vs Range (Continued)

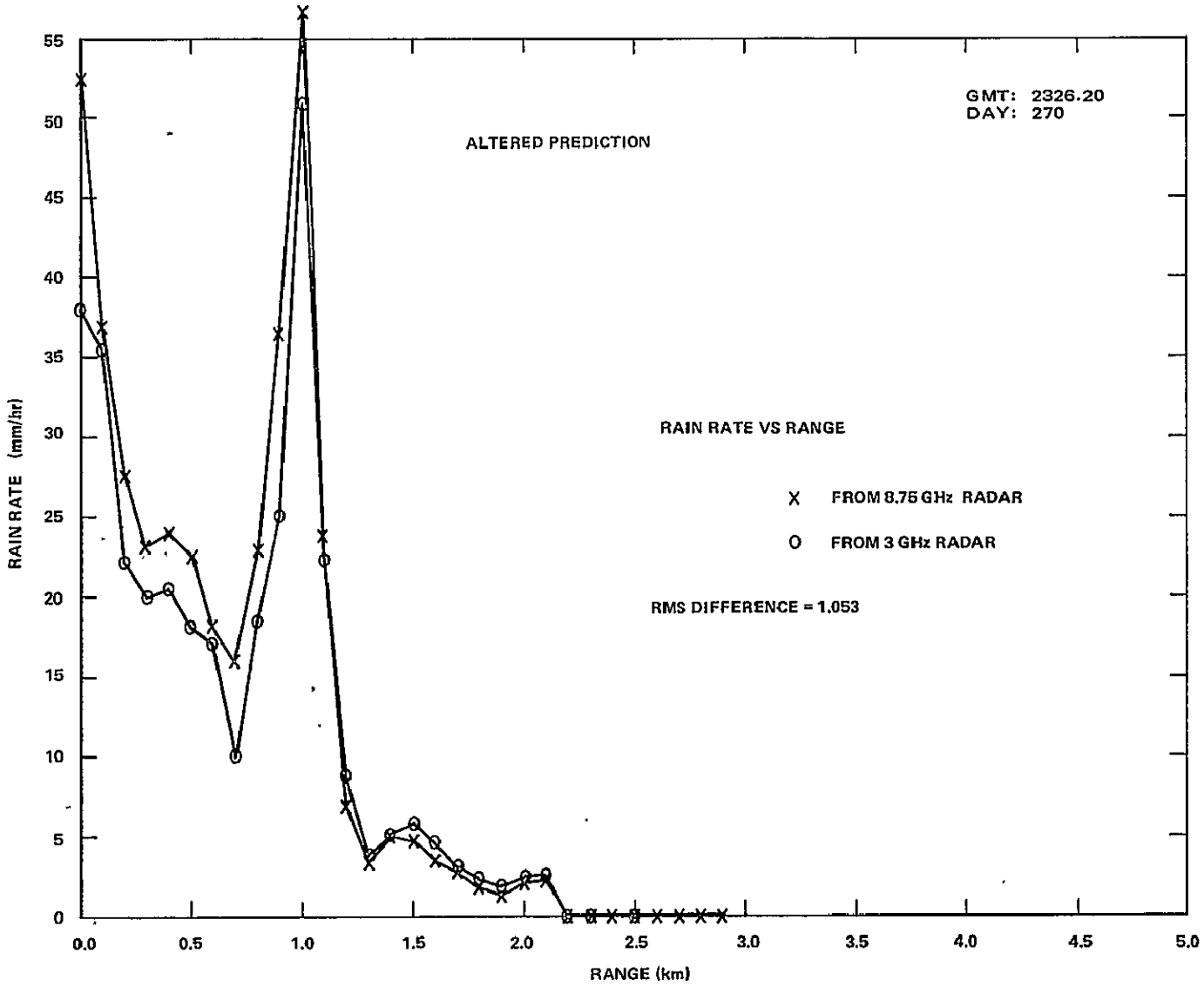

Figure 2. Rain Rates vs Range (Continued)

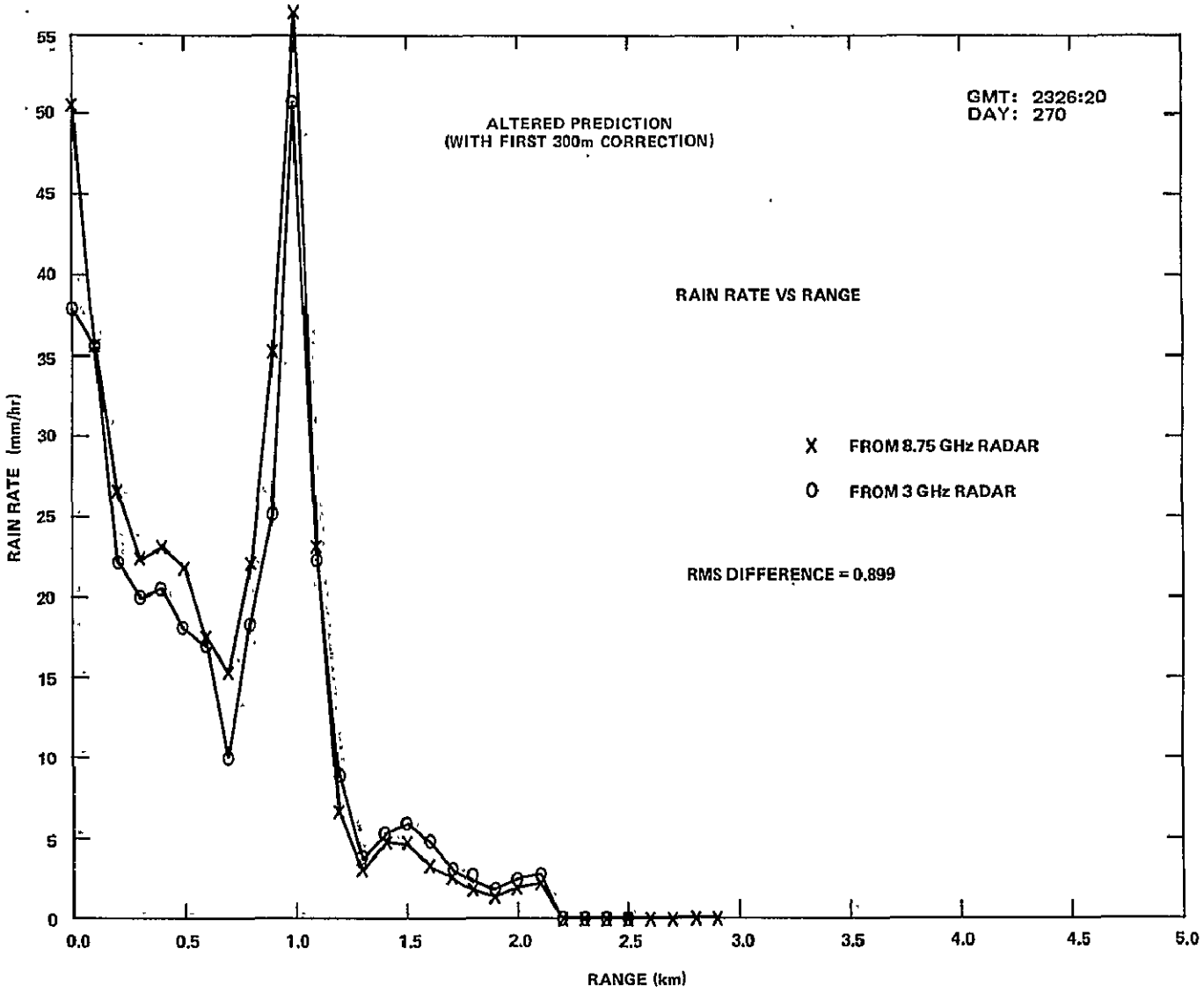

Figure 2. Rain Rates vs Range (Continued)

Table 1

Values of Alpha for $\beta = 0.887$

GMT	Attenuation	Altered Prediction			Standard Prediction		
		3.0 GHz Radar	8 75 GHz Radar	ABS. Difference	3.0 GHz Radar	8.75 GHz Radar	ABS. Difference
2323:20	α(20)	3 607	3.525	082	3.529	4.063	.988
	α(30)	7.256	7 082	.175	7.113	8.101	.534
2324:00	α(20)	3.56	3 54	022	3.56	3.96	.40
	α(30)	7.19	7.15	.047	7.19	7.95	.75
2325.20	α(20)	3 287	3.829	.542	3.218	4.073	.856
	α(30)	6.51	7.48	.968	6.388	7 927	1.539
2326·20	α(20)	3.178	3 653	.475	3.079	3.738	659
	α(30)	6 229	7 074	845	6 058	7.225	1.167

The Figure 2 plot labeled Altered Prediction (with first 300 m correction) takes into account the attenuation introduced by the rain rate in the first 300 meters along the path. The rain recorded by the rain gauge buckets has been used to predict the added attenuation along the path by

$$k(db) = 0.00657\, R^{1.29} \quad (0.3) \qquad (6)$$

derived in Appendix B.

For rain rates greater than 10 mm/hr in the first 300 m of path length, the improvement is probably significant enough to justify the increase in the necessary computational time. The fact that the radars can not measure the first 300 m out and the errors introduced into the prediction of the downlink attenuation are discussed in the last section of this report.

Although the above procedures seem to produce some improvement, there are several reasons for attempting to calibrate the radars using measured rain rate:

- to confirm or correct the above relations of $Z_3 - R$, $Z_8 - R$
- to find how the Z-R relations vary with rain type
- to compare the measured rain rate with the radar predicted rain rate and adjust the parameters accordingly.

Calibration Procedure

If both radars are pointed in a nearly horizontal direction, x, over the rain gauge buckets then the radar equations become:

$$P_3 = C_3 Z_3 / x^2$$

$$P_8 = \frac{C_8 Z_8}{x^2} 10^{-0.2\int k dx} = \frac{C_8 Z_8}{x^2} e^{-2\int k' dx}$$

where

$$k = 4.343\, k'$$

Taking 10 X log of both sides, solving for dbZ_3 and dbZ_8 and approximating the integral $\int_0^x k\, dx$ by $\sum_{i=1}^{N} k_i$, then at range r_j

$$db\, Z_3(r_j) = dbP_3(r_j) - dbC_3 + 2dbr_j$$

$$db\, Z_8(r_j) = dbP_8(r_j) - dbC_8 + 2dbr_j + 2\sum_{i=1}^{j} k(r_j) \qquad (7)$$

If a measurement of the rain rate is made at r_j by means of rain gauge bucket then

$$R = cZ_3^P$$

$$R = c'Z_8^{P'}$$

or

$$db\ R = dbc + p\ dbZ_3$$

$$db\ R = dbc' + p'dbZ_8 \qquad (8)$$

Combining (6) and (7) gives:

$$dbC_3 = dbP_3(r_j) + 2dbr_j + \left(\frac{dbc - dbRR(r_j)}{P}\right)$$

$$dbC_8 = dbP_8(r_j) + 2dbr_j + \left(\frac{dbc' - dbRR(r_j)}{P'}\right) \qquad (9)$$

$$+ 2 \sum_{i=1}^{j} k(r_i)$$

where $\sum_{i=1}^{j} k(r_i) = k(100) + k(200) + \ldots + k(j \times 100)$

and

k(r) is the one-way attenuation/100 m at range r.

Equation (9) indicates that once a $Z_3 - R$ relation is assumed, the radar constant C_3 can be found. Alternatively, if C_3 and p are assumed, c is computed or if C_3 and c are assumed, p is computed. In general, for the computation of C_8 in (9), some estimate of attenuation must be used, such as (2), although for small range values and rain rates less than 25 mm/hr, the last term on the right side of (7) is negligible and C_8 is amenable to direct computation.

FUNCTIONAL RELATION BETWEEN SURFACE AND ELEVATED RAIN RATES

Experimental Procedure

It was noted previously that rain gauge measurements give a direct record of rain rate on the ground and not along the path of interest. Conventional linear or exponential extrapolation

from ground upward is usually inadequate because of the temporal and spatial variations of rain. Applicable experimental and theoretical methods are developed herein in order that more accurate reconstructions of rain rate at elevated heights can be made.

The measurement procedure, which is a slight variation of the calibration technique described previously, employs two radars. One looks along the horizontal over the rain gauge buckets while the other looks along various elevation angles.

The radar equations can be written as:

$$P_1(r) = \frac{C_1 Z_1}{r^2} e^{-2\int k_1' dr} = \frac{C_1 Z_1}{r^2} 10^{-0.2\int k_1 dr}$$

$$P_2(r) = \frac{C_2 Z_2}{r^2} e^{-2\int k_2' dr} = \frac{C_2 Z_2}{r^2} 10^{-0.2\int k_2' dr}$$

in which

$$k = 4.843\, k'$$

Assuming that at least one radar is non-attenuating, say radar 2, then:

$$P_{NA}(r) = C_2 Z_2 / r^2$$

Next let the non-attenuating radar be directed along an elevated angle θ and the attenuating radar directed along the horizontal (using the notation at Figure 3) then:

$$P_A(x) = \frac{C_1 Z_1(x,o)}{x^2} e^{-2\int_o^x k_1 dx}$$

$$P_{NA}(r) = \frac{C_2 Z_2(x,h)}{(x^2 + h^2)}$$

Writing:

$$Z_1(x,o) = a_1 R^b(x,o)$$

$$Z_2(x,h) = a_2 R^b(x,h)$$

where a_1, a_2 can be found either by the calibration technique or some suitable empirical formula (Appendix A or B).

Let

$$R^b(x,h) \Big|_{x_o} = R^b(x,o)\, f(h) \Big|_{x_o}$$

where f(h) is the function relating the rain rate at ground (x,o) to the rain rate along the beam at the point (x,h). In general, f(h) will be a function of x and h.

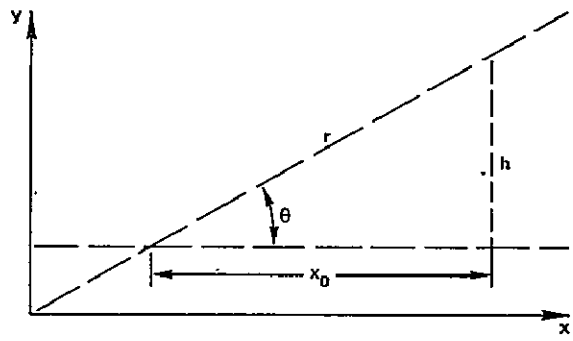

Figure 3. Radar Direction Notation

Combining the above relations substituting in the equations for return power and taking the ratio, then:

$$f(h) \Big|_{x_o} = \frac{C_1 P_2}{C_2 P_1} \quad \frac{a_1}{a_2} \; (1 + h^2/x_o^2)\, e^{-2\int_o^{x_o} k_L dx}$$

An important case occurs when two non-attenuating radars are used in which case $k_L \rightarrow o$ and:

$$f(h)\int_{x_o} = \frac{C_1 P_2}{C_2 P_1}\,\frac{a_1}{a_2}\,(1+h^2/x_o^2)$$

Only when the wavelengths of the two radars are identical can a_1 be set equal to a_2. This case will also occur if the same radar is steered from the horizontal to an elevation angle θ in a time which is less than a significant change in the rain rate. Then:

$$f(h)\int_{x_o} = \frac{C_1 P_2}{C_2 P_1}\,(1+h^2/x^2) = \frac{C_1 P_2}{C_2 P_1}\,\sec^2\theta$$

where

$$(1+h^2/x^2) = \sec^2\theta$$

and θ is as shown in Figure 3.

If the above conditions are not met, i.e. if the same λ is not used or one is at an attenuating λ, then a method is needed to evaluate the attenuation factor $e^{-2\int k\,dx}$. Possibilities include

- Use the theoretical expression for K, either (2) or the one given in Appendix B.
- Use the calibration procedure after first having assumed a $Z_{8.75} - R$ relation.
- Consider:

$$P_1 \doteq \frac{C_1 a_1 R^b(x,o)}{x^2}\,e^{-2\int_o^x k\,dx} \qquad (10)$$

Taking the derivative with respect to range:

$$dP_1/dx = \frac{C_1 a_1 R^b(x,o)}{x^2} \quad e^{-2\int_o^x k\,dx} \qquad (11)$$

$$x\left[-\frac{2}{x} - 2k_L(x) + \frac{1}{R^b(x,o)} \quad \frac{dR^b(x,o)}{dx}\right]$$

Dividing (11) by (10) and using

$$\frac{dP_1/dx}{P_1} = \frac{d \ln P_1}{dx}$$

and

$$k(o) = 0$$

then:

$$\frac{d \ln P_1}{dx} = \left[-\frac{2}{x} - 2k(x) + \frac{d}{dx} \ln R^b(x,o)\right]$$

so:

$$k(x) = \frac{1}{2}\left[\frac{d}{dx} \ln\left[R^b(x,o)\right] - \frac{2}{x} - \frac{d \ln P_1}{dx}\right]$$

and

$$f(h)\Big]_{x_o} = \frac{C_1 P_2 a_1}{C_2 P_1 a_2} \quad (1 + h^2/x_o^2)\, e^{-2k(x)x_o}$$

Thus, f(h) depends on the ground rain rate (through the factor of k(x)). This rain rate, R(x,o), can be found by rain gauge buckets positioned at x and $x + \Delta x$.

These equations follow a procedure similar to that given by Goldhirsh and Katz[10,11,12]. The accuracy of such techniques, however, at the frequencies 3.0 and 8.75 GHz do not seem to warrant the labor involved. The first two procedures, therefore, are preferable.

Theoretical Procedure

A recent personal communication[7] concerning a presentation of the 1975 URSI meeting[8], describes a computational technique for relating ground to height rain rate:

Let the rain rate be recorded on the ground at times $t_1, t_2, \ldots t_k$. The problem is to find the rain rate at height h at some previous time t_o. By means of the Laws and Parsons drop size distribution, the percentage of the total water volume contributed within a certain diameter increment is known. The number density for a given ground rain rate is given by

$$N_D = Rp/1.885 \times 10^4 \nu D_i^3$$

where: N_D = density of drops centered about a particular drop size D_i.

R = rain rate

ν = velocity of drops of size D_i.

p = percent of total water volume consisting of drops centered about a particular drop size D_i.

Consider the ground rain rate recorded at time t_i. Then, at the height h and at the previous time of interest, t_o, the velocity of those drops centered about a diameter D_i (assuming terminal velocity of drops from y = h to y = 0) is given by

$$\nu(D_i) = h/(t_i - t_o)$$

If v (D_i) is a known, single-valued function of D_i (Medhurst[1]) then the inverse exists:

$$v_i = f(D_i) \text{ or } D_i = f^{-1}(v_i)$$

Since the rain rate at time t_i has been recorded, the density of these drops of diameter D_i can be found. Assuming that no change in the drop size structure occured during the drop's downward course, then this is the same density that existed at height h at the previous time, t_o.

Similarly for the ground rain rate at another time t_j,

$$v(D_j) = h/(t_j - t_o)$$

and

$$D_j = f^{-1}(v_j)$$

From the ground rain rate at time t_j this density is found of these drops centered about D_j and hence the density at $y = h$, $t = t_o$.

The entire drop size distribution can be reconstructed at height h and time t_o. Assuming that the drops have reached terminal velocity at height h then the rain rate can be computed

$$R(y=h, t=t_o) = \frac{\pi}{6} \sum_{i=1}^{N} D_i^3 N_D(D_i, h) v_t(D_i, h)$$

where N_D (D_i,h) is the density of drops centered about diameter D_i located at the height h and v_t(D_i,h) is the terminal velocity of drops D_i at height h.

Several criticisms can be made of this technique. It is not evident that the terminal velocities of drops can be used for drops falling from height h to ground. Furthermore, the expressions for terminal velocity assume the absence of updraughts—an assumption which is usually not the case especially in severe storms. For cross winds, it is necessary to compensate for the horizontal displacement of drops as they fall.

Despite these problems, the technique seems to be more rigorous and potentially more accurate than the usual time shift and linear extrapolation used to relate ground to elevated rain rates. Correctional procedures, such as directional anemometers placed near the rain gauge buckets, along with the use of radar as described in "Calibration Techniques" herein may be possible.

Some preliminary results are given in Figures 4 and 5. The reconstructed rain rates (solid unmarked lines) have been superimposed upon Westinghouse curves of rain rate vs. time as given by the ground rain buckets (solid curves with crosses) and the appropriate radar bin predictions[4] (dotted curves), i.e. that radar bin at a height h directly over the rain gauge bucket. The radar data given in the Figure 4 was taken at a height of 884 m. It should be noted that the reconstructed rain rate differs markedly from a time-shifted version of the original ground rain rate curve. Figure 5, plotted at 330 m, shows less-pronounced difference; a reflection of the fact that total drop size structure for smaller heights approaches the structure at ground level. Since the data were taken during a fairly intense storm some measurement of updraught and cross wind velocities would be needed for a more accurate reconstruction. One other possible procedure for improving accuracy is by the use of the terminal velocities of rain drops aloft.[9] It is expected that the accuracy of this reconstruction technique will improve as the amount of reliable information input to the model increases.

TWO-FREQUENCY RADAR TECHNIQUES

Goldhirsh-Katz Method

A series of articles[10,11,12] by Goldhirsh and Katz outline how various storm and radar

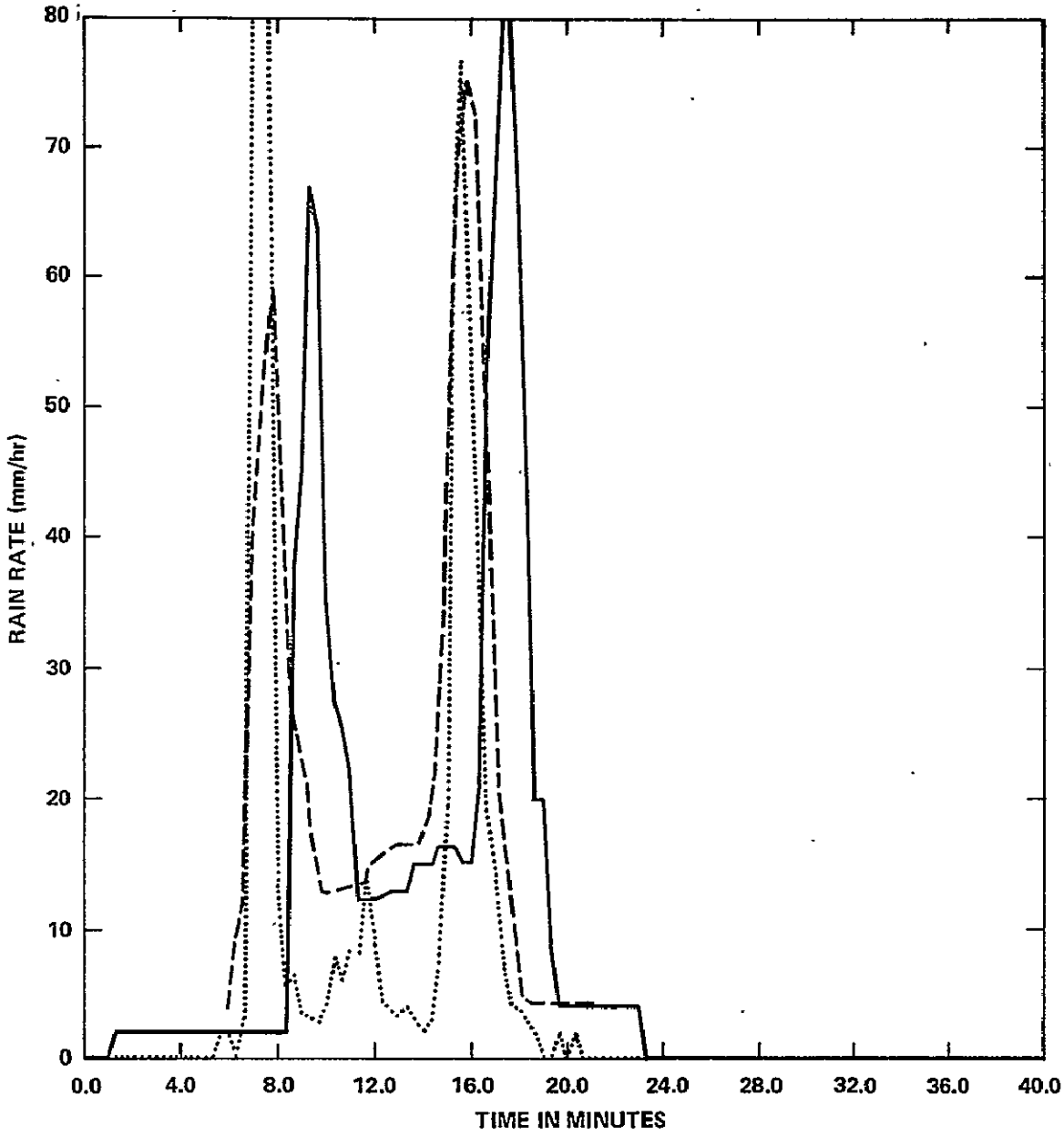

START TIME	STOP TIME
YEAR = 74	YEAR = 74
DAY = 270	DAY = 270
GMT = 910	GMT = 1940

NO SECS AVGD = 20

····· RANGE BIN 24

——— RAIN BUCKET 10

— — — — RECONSTRUCTED RAIN RATE

Figure 4. Rain Rate vs Time at 884 Meters

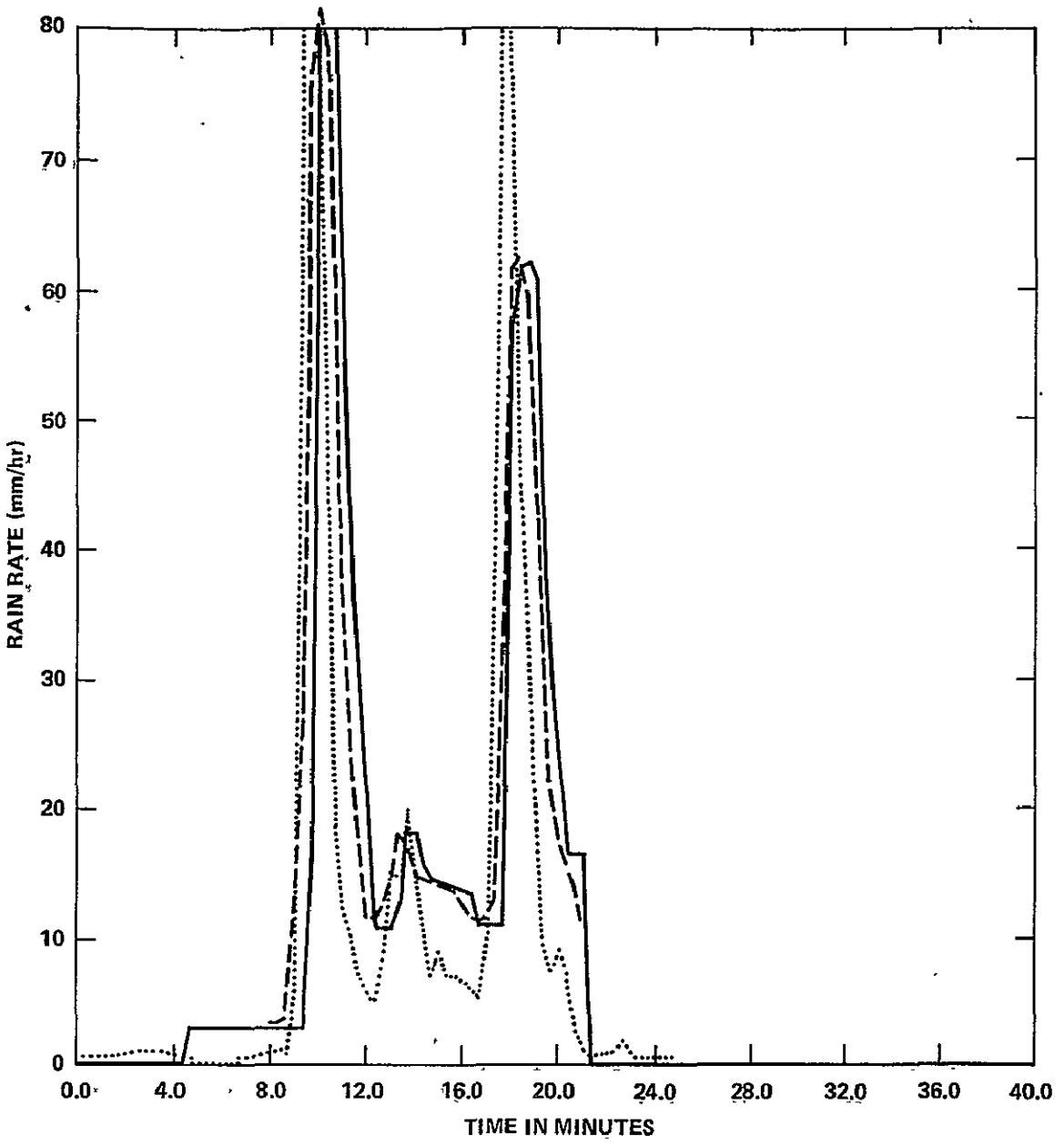

Figure 5. Rain Rate vs Time at 330 Meters

parameters can be derived through the use of a multifrequency radar system. In a two frequency system consisting of an attenuating and non-attenuating radar, the average attenuation within a certain range interval is found to be essentially a ratio of radar return powers measured at the end points of this interval.

The equations that follow are the same as those of Goldhirsh and Katz except for elimination of the assumption that the effective reflectivity factors for the two radars are identical. The only condition necessary is that:

$$b = b'$$

where

$$Z_{NA} = a R^b$$

$$Z_A = a' R^{b'}$$

where NA denotes non attenuating
A denotes attenuating

Writing the radar return powers of the two radars at the ranges r and r + s

$$P_{NA}(r) = C_2 Z_{NA}(r)/r^2 \tag{12}$$

$$P_A(r) = \frac{C_1 Z_A(r)}{r^2} \cdot 10^{-0.2\int_0^r k dr} \tag{13}$$

$$P_{NA}(r+s) = \frac{C_2 Z_{NA}(r+s)}{(r+s)^2} \tag{14}$$

$$P_A(r+s) = \frac{C_1 Z_A(r+s)}{(r+s)^2} \; 10^{-0.2\int_o^{r+s} k\,dr} \tag{15}$$

Dividing (12) by (13) taking 10 X log of the resultant and using the relations $Z_{NA} = a_2 R^b$ and $Z_A = a_1 R^b$

then:

$$10 \log\left[\frac{P_{NA}(r)}{P_A(r)}\right] = 10\left[\log\left(\frac{C_2}{C_1}\right) + \log\left(\frac{a_2}{a_1}\right) + 0.2\int_o^r k dr\right] \tag{16}$$

Proceeding similarly with (14) and (15)

$$10 \log\left[\frac{P_{NA}(r+s)}{P_A(r+s)}\right] = 10\left[\log\left(\frac{c_2}{c_1}\right) + \log\left(\frac{a_2}{a_1}\right) + 0.2\int_o^{r+s} k dr\right] \tag{17}$$

Subtracting (16) from (17) and approximating $\int_r^{r+s} k\,dr$ by $\bar{k}s$ where the bar denotes an average, then:

$$\bar{k} = \frac{1}{2s}\left[dbP_{NA}(r+s) - dbP_{NA}(r) + dbP_A(r) - dbP_A(r+s)\right] \tag{18}$$

where s is expressed in km and $\bar{k}$ is the average attenuation in the interval s in db/km.

The advantages of equation (18) are the independence of $\bar{k}$ on the radar calibration constant and the absolute range, (i.e. only the increment length s enters in). The results are due to the fact that $\bar{k}$ is sensitive only to return power changes in the interval (r, r + s). One other

advantage of the method is that if the exponents in the Z-R relation are taken to be equal, ($b = b'$), then $\overline{K}$ is also independent of the coefficients a_1 and a_2 in the Z-R relations.

The drawback of this and similar techniques are the errors arising from the statistical nature of the target. The fluctuations are caused by changes in the relative positions of the particles (i.e. positional changes of a significant part of the radar wavelength) and result in variations of the incoherent addition of backscattered powers from the individual scatterers. Such changes occur in times on the order of milliseconds.

Among the parameters necessary for the determination of the error variance of Z are the signal to noise ratio and the number of dependent samples used to estimate Z[14]. It should be noticed that for a given Z value the errors will depend upon range and attenuation as well as the magnitude of Z as these quantities determine the backscattered signal level.

For an estimate of the number of independent samples taken by the radars, an equation from Battan is used

$$\tau_{.01} = 1.71 \times 10^{-3} \text{ sec}$$

where $\tau_{.01}$ is the time required for the autocorrelation of the signal to fall to 01.

For the Rosman radars, the averaging is done over 1.8 sec at a PRF = 1 KHz. Therefore, for the 3 & 8.75 GHz radars 105 and 307 independent samples, respectively, are obtained per range bin out of a total of 1800 return pulses. Noise level inputs to the preamp are –102 dbm and –99.5 dbm for the 3 and 8.75 GHz radars respectively, while the signal levels are found from the standard radar equations.

Statistical analyses required to complete error variances of reflectivity and rain rate or to assess the viability of multi-frequency radar techniques could not be included in this report. Nevertheless, it is suggested that statistical analyses be taken as an essential part of future radar data processing.

The method used to analyze the ATS-6 data using the Golhirsh-Katz method is given below.

For a given increment length S, equation (18) is used to compute attenuation, using an average of three data points as estimates of return power at the ends of the interval. Next, the average dbZ_3, value within the increment S is computed. As a result, pairs of values (k, dbZ) are found throughout the entire data set of radar return power vs range.

The final step is finding the average and variance of those values of k which correspond to dbZ values falling in some ΔdbZ increment centered about a particular dbZ. The entire process is repeated for various incremental lengths S ranging from 0.5 to 1.3km. Some of the results are contained in Table 2 below in tabular form where the values of k as computed by the Goldhirsh-Katz method are compared with values of k (in db/km) computed by the method of Appendix B.

Table 2

Comparative Attenuation Results

DAY: 270 GMT. 2325:20 S = .9 km

DBZ_{AV}	k (Goldhirsh-Katz)	k $= 0.00029 Z^{.72}$	k $= 0.00004 Z^{.857}$
39.9	0.156	0.22	0.141
40.4	0.177	0.235	0.153
40.7	0.138	0.247	0.163
41.3	0.433	0.273	0.184
41.5	0.242	0.283	0.193
42.6	0.997	0.339	0.24
42.8	0.285	0.349	0.249
43.25	1.12	0.377	0.247
43.7	0.339	0.406	0.30
44.1	0.368	0.432	0.325

General characteristics of the results are:

- As S increases, for a given number of points averaged, the variance of k decreases.
- Although the results show that an increase in dbZ is usually accompanied by an increase

in k, for a significant portion of the data k is not a monotonically increasing function of dbZ.

- For the data analyzed here the Goldhirsh-Katz method usually predicts a larger value of k than the theoretical formulas.

In the absence of an adequate error analysis, the accuracy of the Goldhirsh-Katz technique is difficult to assess. In general, the predictions are larger than those given by the theoretical formulas. Figure 1 demonstrates that if the 8.75 GHz calibration constant is decreased, the 8.75 GHz signal attenuation must increase for proper agreement of predicted rain rates. That the 8.75 GHz calibration constant may be too large can be seen from the curves at Figure 6 which compare ground rain rate with the corresponding 8.75 GHz predictions. The height difference between rain bucket and range bin is fairly small, i.e. 102 m so a correlation coefficient near 1 is expected. It should be kept in mind, however, that for the computation of the rain rate, the same Z-R relation ($Z = 200\ R^{1.6}$) was used throughout.

In addition to experimental measurements of attenuation, Goldhirsh and Katz demonstrate that, in principle, an estimate of drop size distribution can be found by employing an attenuating and non-attenuating radar. Once this distribution is known over the path of the downlink signal, the expected attenuation of the 20 and 30 GHz downlinks can be computed without having to deal with the intermediate quantity of rain rate.

Assuming the Marshall-Palmer form for the drop size distribution,

$$n(D)\,dD = n_o e^{-\Lambda D}\,dD \tag{19}$$

and

$$Z_{NA} = \int_o^\infty \delta_{NA}(D)\, n(D)\, D^6\, dD \tag{20}$$

and

$$k = \int_o^\infty C_{ext}(D)\, n(D)\, dD \tag{21}$$

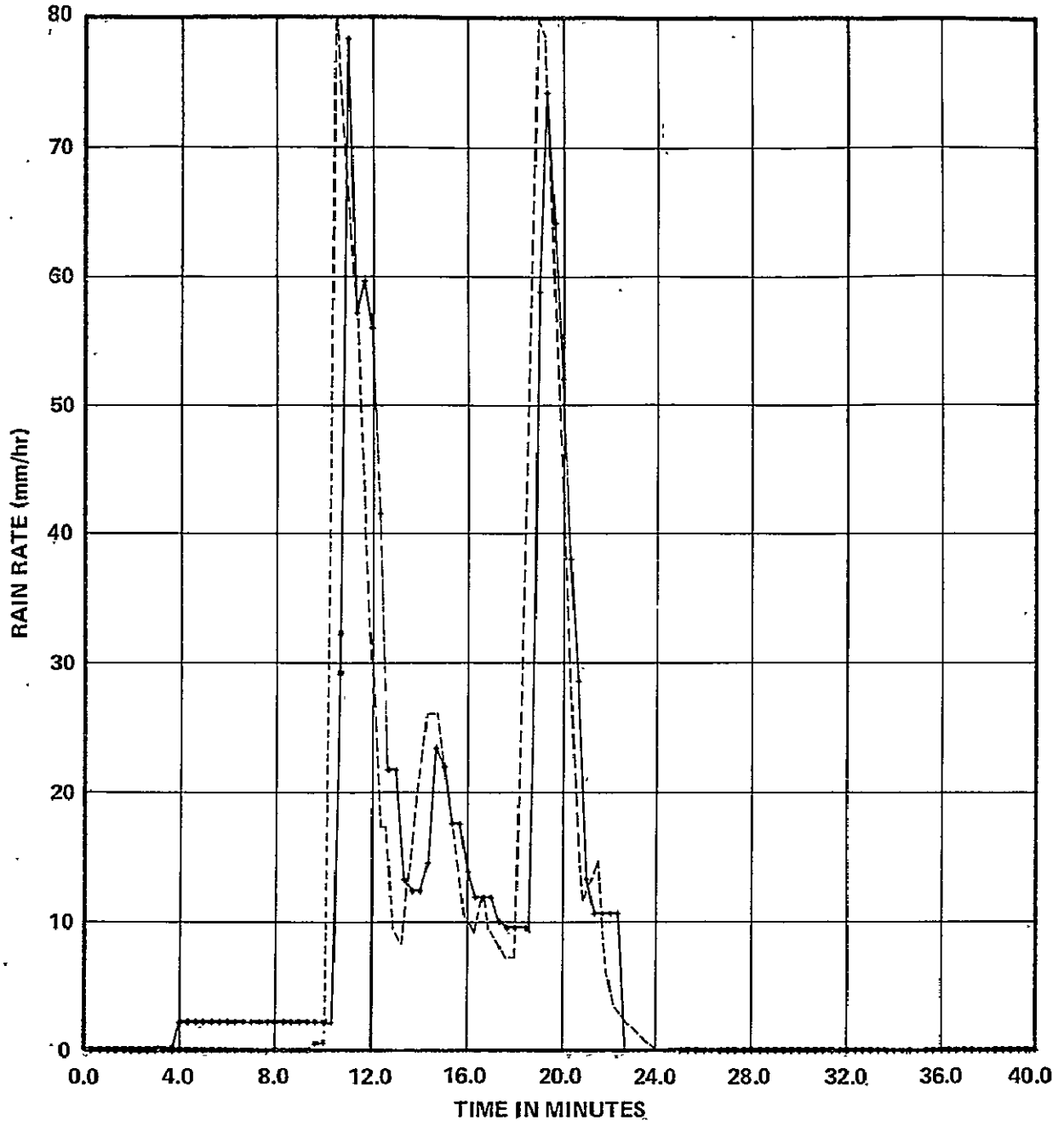

START TIME	STOP TIME
YEAR = 74	YEAR = 74
DAY = 270	DAY = 270
GMT = 1910	GMT = 1940

NO SECS AVGD = 20

--------- RADAR BIN = 1

———— RAIN BUCKET = 2

Figure 6a. 3.0 GHz Radar vs Rainbucket Rain Rate

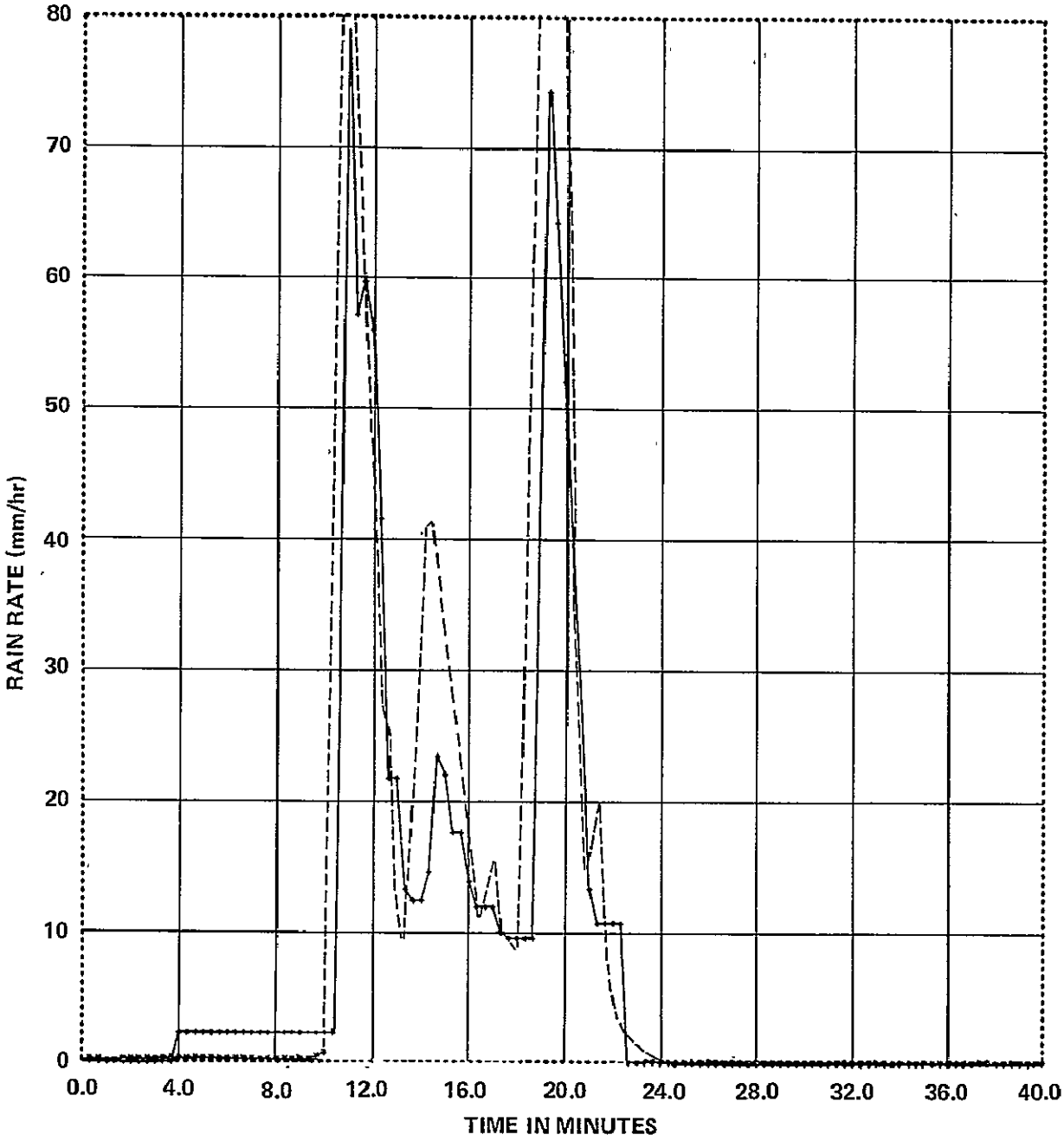

Figure 6b. 8.75 GHz Radar vs Rainbucket Rain Rate

and taking the ratio k/Z_{NA} and using equations (19), (20), and (21) then

$$\frac{k}{Z_{NA}} = \frac{\int_o^\infty C_{ext}(D)\, e^{-\Lambda D} dD}{\int_o^\infty \sigma_{NA}(D)\, e^{-\Lambda D} D^6 dD} \tag{22}$$

where Z_{NA} is given by equation (12), k by equation (18) and values of $C_{ext}(D)$, $\sigma_{NA}(D)$ obtained from numerical computations using Mie scatter theory.[1,2]

Equation (22) can be solved numerically for Λ which, in turn, is used to compute n_o through equation (20)

$$n_o = Z_{NA} \Big/ \int_o^\infty \sigma_{NA}(D)\, e^{-\Lambda D} D^6 dD \tag{23}$$

In a recent report on error analysis of this technique[13], an analytic expression is used to approximate (22) and (23) for two radars at 3 and 10 GHz. It is found that:

$$\Lambda(cm^{-1}) = \exp\left[133.094 - 54.267\, x \quad 7.4182\, x^2 - 0.3322\, x^3 \right] \tag{24}$$

and

$$n_o = \eta_{NA} / \exp\left[12.95 - 6.16 \ln \Lambda - 0.1132 (\ln \Lambda)^2 \right] \tag{25}$$

where

$$x = \ln\left(\frac{k}{\eta_{NA}} \right)$$

From Battan[5], pg 44, Z_e, the effective reflectivity factor, is related to η, the reflectivity, through the equation:

$$Z_e = \lambda^4 \eta / \pi^5 |K|^2$$

where

$$|k|^2 = \frac{m^2 - 1}{m^2 + 2} \approx 0.93$$

m = complex index of refraction for water

λ = radar wavelength

for

$$\lambda_3 = 10 \text{ cm}$$

$$\eta_{NA} (km^{-1}) = Z_3 \times (2.846 \times 10^{-9})$$

where Z_3 is in units of mm^6/m^3

$$x = \ln\left(\frac{k}{Z_3}\right) + 19.677$$

If a Z-R relation is assumed, such as the one given in Appendix A,

$$R = (Z_3/261)^{2\beta},$$

then N_D vs D can be plotted for various values of rain rate and attenuation, k. Since the Goldhirsh-Katz method provides neither a convenient analytic representation of k nor reliable values of it for radar frequencies of interest unless a considerable amount of averaging is used, an alternative approach to finding attenuation is considered in the following section.

Alternative Technique

For the experimental determination of radar attentuation, a procedure somewhat different from the Goldhirsh-Katz technique is considered. The motivation is that the predicted rain rate from each of the two radars should be the same and that the discrepancy between the predicted values should be assigned to the selective attenuation of the higher frequency radar. Equating rain rates, or equivalently, 10 log R,

$$10 \log R_3 = 10 \log R_8$$

$$10 \log(aZ_3^b) = 10 \log (a'Z_8^{b'})$$

or

$$10 \log\left(\frac{a}{a'}\right) + 10 \cdot b \cdot \log Z_3 = 10 \cdot b' \cdot \log Z_8$$

If $b = b'$, then, at a single range cell

$$K + dbZ_{3j} = dbZ_{8_j} \tag{26}$$

where

$$K = 10 \log\left(\frac{a}{a'}\right) / b$$

The actual value of dbZ_8 is the sum of the 'measured' dbZ_8 plus the amount of attenuation suffered through the two-way path, where the 'measured' and actual values of dbZ_8 are defined by

$$P = \frac{CZ_8}{r^2} \, 10^{-0.2 \int_0^r k \, dr} = \frac{CZ_{8m}}{r^2}$$

in which the subscript 'm' denotes measured. Taking 10 × log of each of these equations and subtracting one from the other

$$dbZ_{8_j} = dbZ_{8mj} + 2 \sum_{i=1}^{j} k_i \tag{27}$$

where

$$\int_0^r kdr \approx \sum_{i=1}^{j} k_i$$

Relating k_i to Z_3 by the equation

$$k = \alpha Z_3^{\beta}$$

equation (27) becomes:

$$dbZ_{8_j} = dbZ_{8mj} + 2 \sum_{i=1}^{j} \alpha Z_{3i}^{\beta}$$

Equation (26) can be rewritten as:

$$K + dbZ_{3j} = dbZ_{8mj} + 2 \sum_{i=1}^{j} \alpha Z_{3i}^{\beta}$$

This equation characterizes one range bin. For N range bins, N equations result which, when added, give:

$$NK + \sum_{j=1}^{N} dbZ_{3j} = \sum_{j=1}^{N} dbZ_{8mj} + 2\alpha \sum_{j=1}^{N} \sum_{i=1}^{j} Z_{3i}^{\beta}$$

The easiest procedure is to fix β and solve for α from which:

$$\alpha = \frac{NK + \sum_{j=1}^{N} (dbZ_{3_j} - dbZ_{8mj})}{\sum_{j=1}^{N} \sum_{i=1}^{j} Z_{3i}^{\beta}} \qquad (28)$$

Note that for computational ease the denominator can be written

$$\sum_{j=1}^{N} \sum_{i=1}^{j} Z_3^{\beta} = NZ_{3_1}^{\beta} + (N-1)Z_{3_2}^{\beta} + (N-2)Z_{3_3}^{\beta} + \ldots + Z_{3_N}^{\beta}$$

$$= \sum_{k=1}^{N} (N-k+1) Z_{3_k}^{\beta}$$

The attenuation becomes

$$\bar{k} = \alpha Z^{\beta} \qquad (29)$$

where α is given by equation (28).

Equation (29) can be interpreted as the attenuation of the 8.75 GHz signal such that the average absolute difference in the predicted rain rates is minimized. Unlike the Goldhirsh-Katz equation, which computes attenuation in an interval, equations (28) and (29) characterize the set of data points as a whole. Another difference between the two methods is that α, and hence k, depend upon the Z-R relation; a relation which depends upon the radar calibration constants. Nevertheless, this technique is an easy means of comparing the theoretical expressions for attenuation with an expression found from the data. If such a procedure is carried out over a sufficient amount of radar data, characteristic values of α are found for a number of different classes of rain.

Computed values of α are tabulated in Table 3, in which

$$\bar{k} = \alpha Z^{0.88}$$

These values of α should be compared with the theoretical expressions

$$\bar{k} = 0.00004\ Z^{0.88}$$

and

$$\bar{k} = 0.00029\ Z^{0.72}$$

The sharp decrease in alpha between times 2324:10 and 2324:30 corresponds to a fairly rapid movement of the storm towards the receiver, a general increase in rain intensity in the near range cells, and a decrease in the spatial extent of the storm. The increase around GMT = 2328 corresponds to a decrease in rain intensity with the spatial extent of the storm basically unchanged. From time 2324:30 to 2327:50, the computed values are in fair agreement with the theoretical value of 4×10^{-5}. For the remaining intervals 2323:10 to 2324:10 and 2328:10 to 2329:50, the value are greater than two and in some cases as large as three times that given by theory.

Table 3

Phase Changes in Different Rain Rates

GMT	ALPHA	GMT	ALPHA
2323:10	.000129	2326:10	.0000634
2323:30	.000113	2326:30	.0000408
2323:50	.000123	2326:50	.0000457
2324:10	.0000989	2327:10	.0000336
2324:30	.0000523	2327:30	.0000535
		2327:50	.0000635
2324:50	.0000431	2328:10	.000107
2325:10	.0000498	2328:30	.0000824
2325:30	.0000355	2328:50	.0000977
		2328:50	.0000977
2325:50	.0000486	2329:30	.0000939
		2329:50	.000129

One should not conclude, however, that the theoretical expressions for attenuation are necessarily in error by taking as evidence the results of both the Goldhirsh-Katz and the present method. In fact, the Goldhirsh-Katz technique often gives highly variable and, therefore, suspect results while the present method might be using incorrect values for the radar calibration constants and therefore also be in error. Even if it is clear that the theoretical formulas underpredict in certain cases, the problem of explaining the mechanism behind such changes in alpha remains unsolved. One possible cause for the variation in alpha may be a shift in the drop size distribution toward larger drop sizes thereby accounting for an increase in attenuation and therefore in alpha. Disdrometer data, along with radar calibration curves should be helpful.

It should be noted that any anamoly in the attenuation data for the 8.75 GHz radar most likely has an analogue in the measured attenuation of the 20 and 30 GHz downlinks. Therefore a proper explanation of the radar attenuation should also help to resolve the discrepancies between the theoretical and measured downlink attenuation.

Having computed several values of α, theoretical drop size distributions can be plotted based on equations (24) and (25). and the Z-R relation $Z_3 = 261\ RR^{1.5}$. Plots of N_D vs D for various values of rain rate and attenuation are presented in Figure 7. Also plotted on each graph is the Marshall-Palmer distribution (solid lines) given by:

$$N_D\ (m^{-3}\ mm^{-1}) = N_o\ e^{-\Lambda D}$$

where

$$\Lambda\ (cm^{-1}) = 41\ RR^{-0.21}$$

$$N_o\ (cm^{-4}) = .08$$

$$D = \text{drop diameter}$$

The rain rates that correspond to the solid lines are 1, 5, 25 and 50 reading up in a counter-clockwise direction. Certain characteristics of the curves seem to be qualitatively correct. For example: (1) increasing attenuation is accompanied by a greater percentage of larger drops. This accounts for attenuation increase because for a given volume of water, the volume composed of larger drops results in more attenuation; (2) N_D decreases exponentially as D increases, and (3) for small D, N_D increases for larger rain rates, which is in agreement with the modified Marshall-Palmer distribution.[5]

A disturbing feature of the curves is that for $\alpha > 0.000042$, the equations predict a greater percentage of larger drops for rain of 25 mm/hr than at 50 mm/hr. One possible reason is that $\alpha > 4 \times 10^{-5}$ is outside the region of validity for the expressions used. For $\alpha < 4 \times 10^{-5}$ the curves appear qualitatively plausible and it might be of interest to compare height corrected disdrometer data with curves such as those given here.

Due to calibration errors and the statistical fluctuations of scattering from hydrometers, accurate drop size distributions from radar measurements probably cannot be obtained without going to a higher frequency radar. Nevertheless, experiments or error analyses would be of interest not only because of the theoretical importance of such techniques but also for assessing the feasibility of a higher frequency radar for future systems.

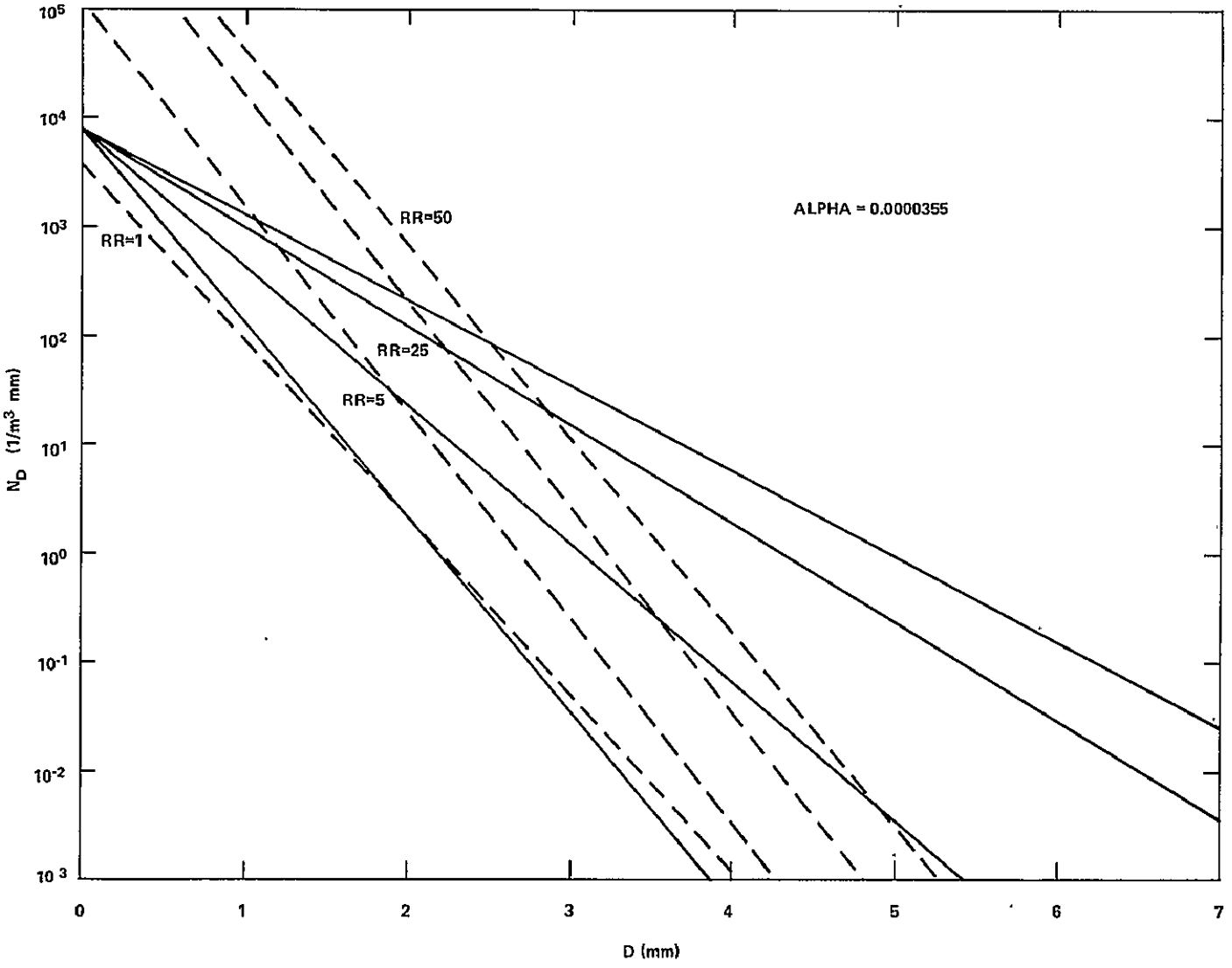

Figure 7. Rain Rate vs Drop Size

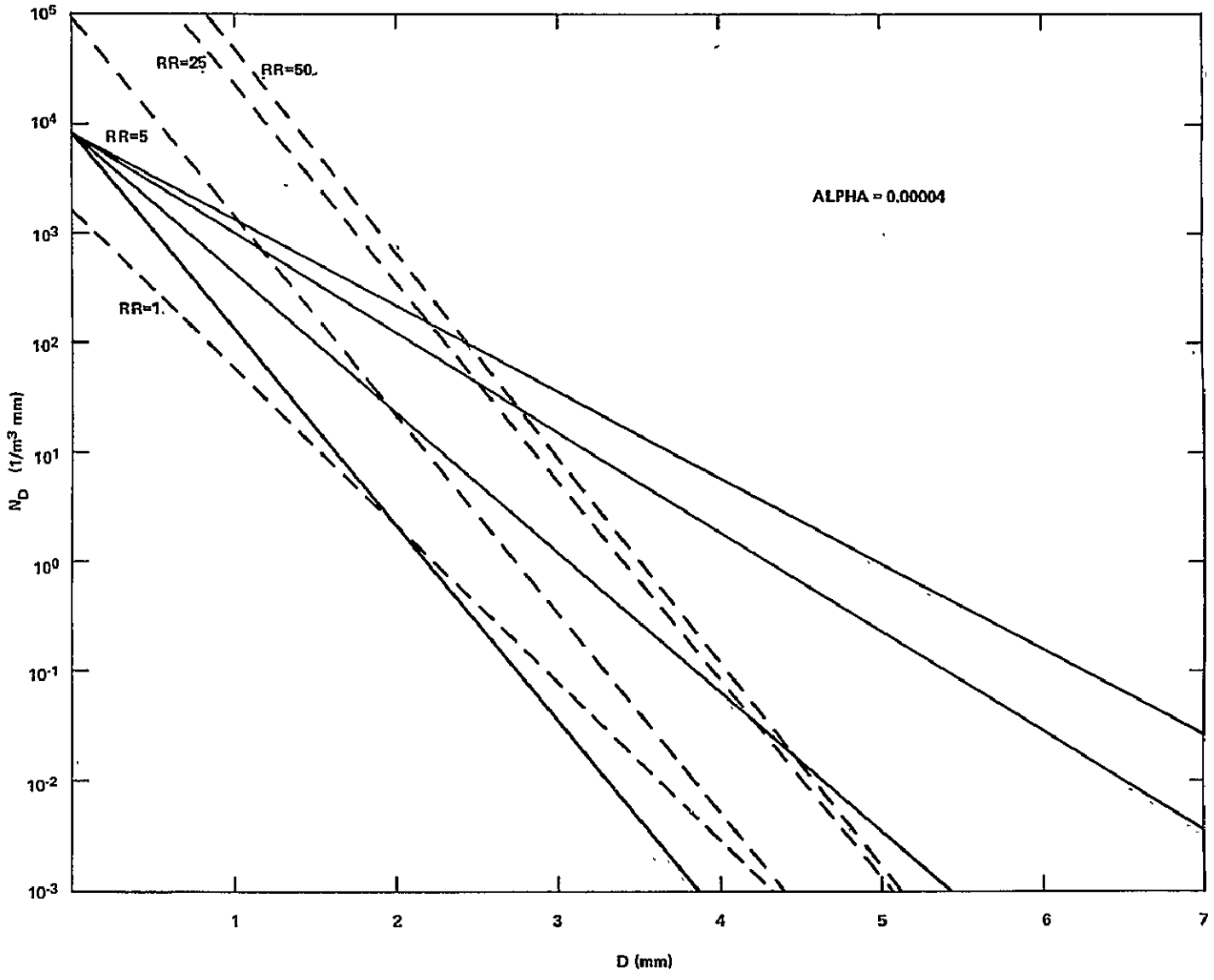

Figure 7. Rain Rate vs Drop Size (Continued)

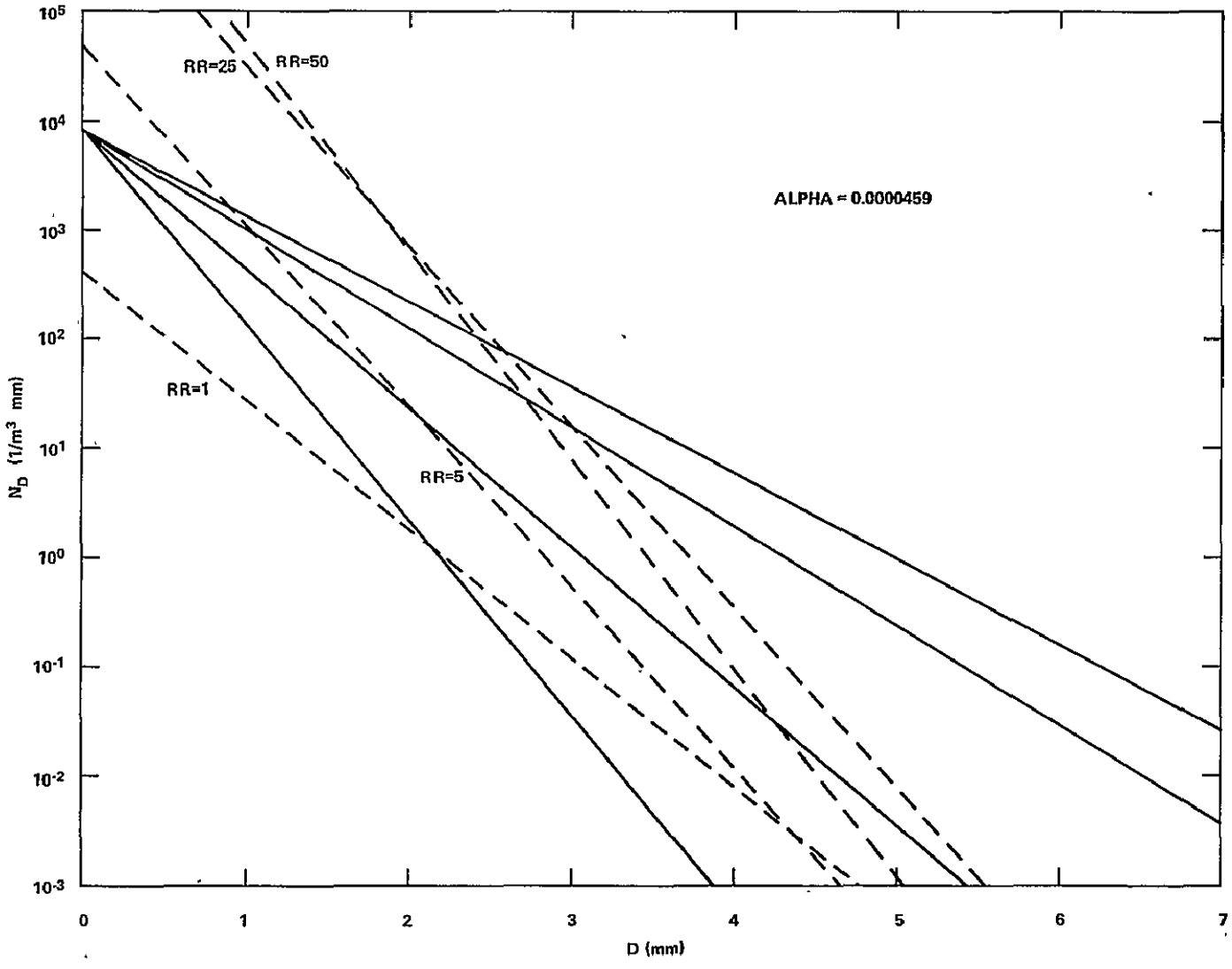

Figure 7. Rain Rate vs Drop Size (Continued)

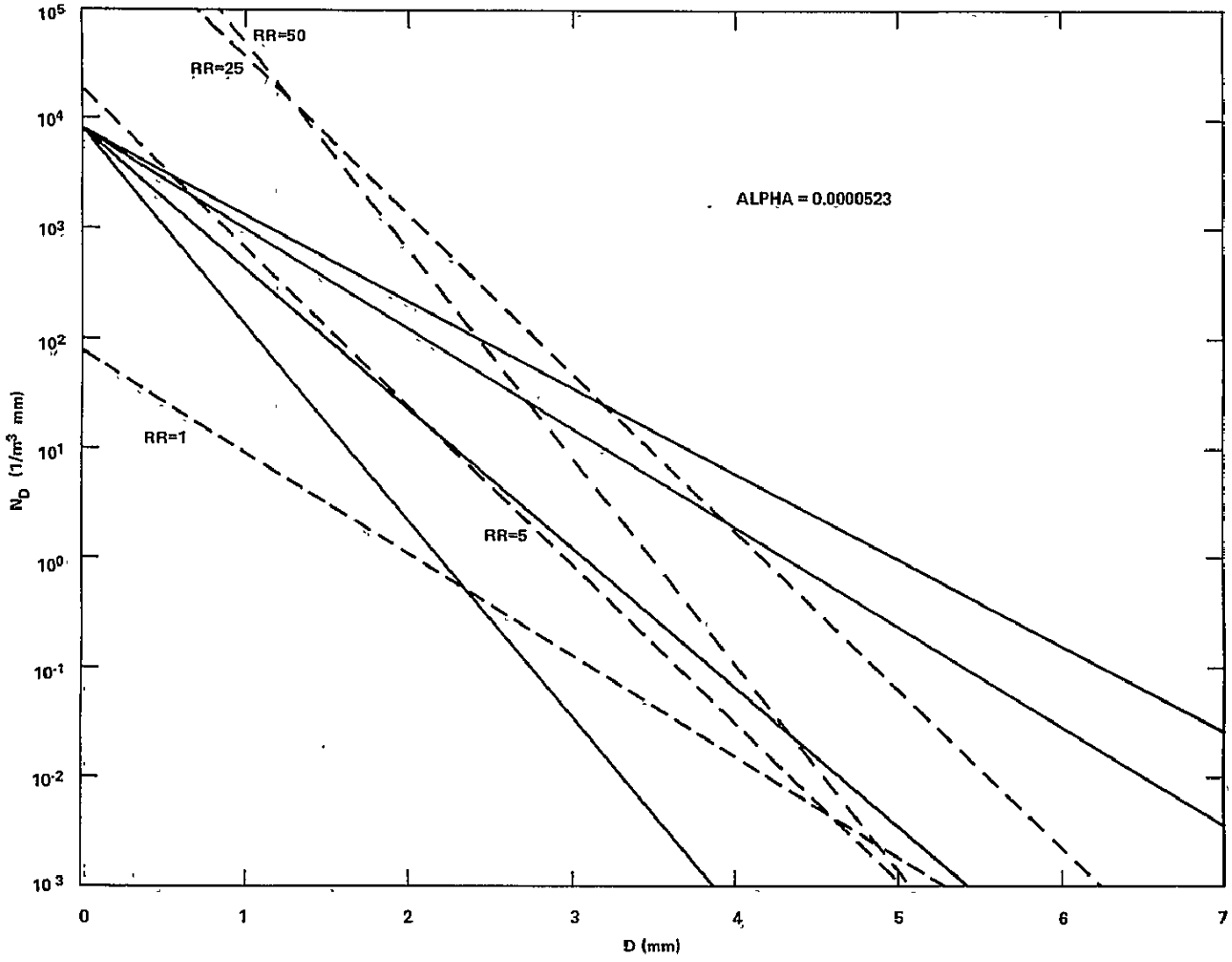

Figure 7. Rain Rate vs Drop Size (Continued)

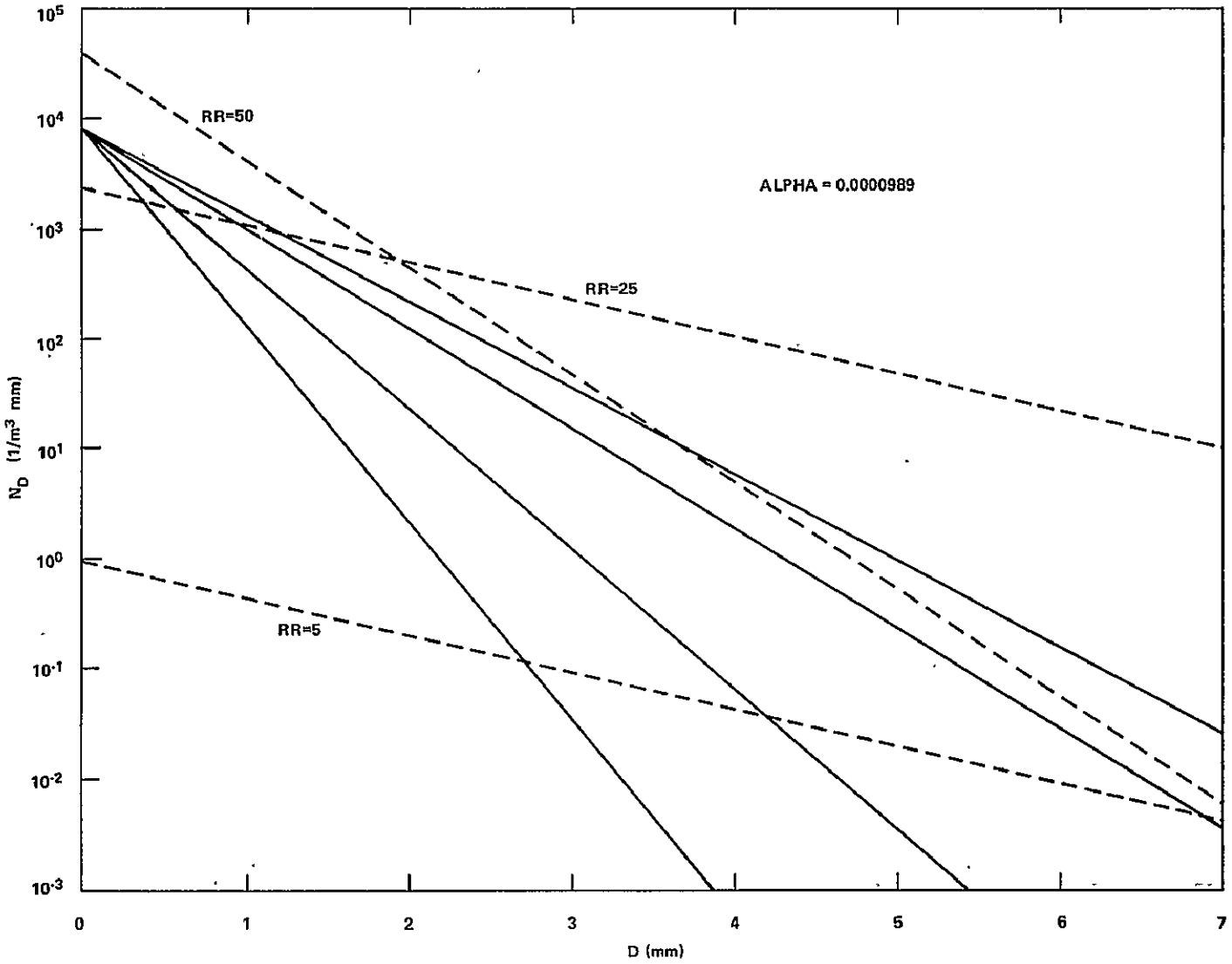

Figure 7. Rain Rate vs Drop Size (Continued)

PHASE DIFFERENCE INFORMATION RELATED TO METEOROLOGICAL PARAMETERS

At Rosman, differential phase measurements are made between the carrier and various side tones. The question of interest is how this quantity varies with the meteorological conditions along the downlink path. The procedure, following Van de Hulst[15], uses an effective refraction index to characterize forward scattering through a multi-particle region.

Van de Hulst considers a slab of length ℓ filled with N particles/vol, identical and identically oriented. The distance Z from the observation point to the slab is assumed to be much larger than a wavelength, λ. Further, if the effective refractive index is such that $\tilde{m} \approx 1$, then the ratio of total to incident disturbance is:

$$\frac{u}{u_o} = e^{-ik\ell(\tilde{m}-1)} = \left\{1 - \frac{2\pi}{k^2} N\ell S(0)\right\}$$

let

$$\tilde{m} = n - in'$$

then

$$e^{-ik\ell(\tilde{m}-1)} \approx 1 - ik\ell(\tilde{m} - 1) = 1 - ik\ell(n - in' - 1)$$

Therefore

$$n = 1 + 2\pi N k^{-3} \operatorname{Im}\left\{S(0)\right\} \qquad (30)$$

where S(o) denotes the amplitude scattering factor in the forward direction.

Equation (30) determines the phase lag of the wave. The effect of such a phase lag, as Van de Hulst remarks, is a dispersive medium characterized by a wave velocity v, where $v = c/n$.

If the particles have a distribution of radii given by N(a), then:

$$\tilde{m} = n - in' = 1 - \frac{i2\pi}{k^3} \int S(o, a) N(a)\, da$$

and

$$n = 1 + \frac{2\pi}{k^3} \int_0^\infty \mathrm{Im}\left\{ S(o,a) \right\} N(z,a)\, da$$

The drop size dependence on z is used simply to emphasize the spatial variation of the distribution. The quantity S(o,a) can be related to the Mie scatter coefficients by

$$S(o,a) = \frac{1}{2} \sum_{n=1}^{\infty} (2n+1)(a_n + b_n)$$

so that:

$$n = 1 + \frac{\pi}{k^3} \int_0^\infty \sum_{n=1}^{\infty} (2n+1)\, \mathrm{Im}\,(a_n + b_n)\, N(z,a)\, da \qquad (31)$$

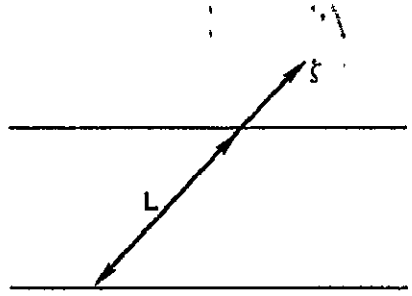

Figure 8. Notation for Path Length

Referring to Figure 8 and using the relation

$$n = c/v = c/d\zeta/dt$$

then

$$t = \frac{1}{c} \int_0^L n(\zeta)\, d\zeta \qquad (32)$$

Substituting equation (31) into (32):

$$t = \frac{L}{C} + \frac{\pi}{ck_o^3} \int_0^L \int_0^\infty \sum_{n=1}^{\infty} (2n+1)\, \mathrm{Im}(a_n + b_n)\, N(z,a)\, da\, d\zeta \qquad (33)$$

The phase of the wave can be written:

$$\varphi = 2\pi(t/T);\ T = \text{period}$$

For the ATS-6 Millimeter Wave experiment, three monochromatic signals are sent in phase from the spacecraft. The quantity measured at the ground station is:

$$\varphi_d = \varphi_u + \varphi_L - 2\varphi_c$$

Where the subscripts C, U, L denote the carrier and the upper and lower sidebands.

For clear sky measurements, the above quantity is calibrated to zero:

$$\varphi_{dNR} = 2\pi\left(\frac{t'_u}{T_u} + \frac{t'_L}{T_L} - \frac{2t'_c}{T_c}\right) \rightarrow 0 \tag{34}$$

Using equation (34), the differential phase measured in rain can be written:

$$\varphi_{dR} = 2\pi\left[\frac{(t_u - t'_u)}{T_u} + \frac{(t_L - t'_L)}{T_L} - \frac{2(t_c - t'_c)}{T_c}\right] \tag{35}$$

which is just the phase lag measured with respect to clear sky conditions. Using equation (32) gives:

$$\varphi_{dR} = \frac{2\pi^2}{T_u c k_{o_u}^3} \int_o^L \int_o^\infty \sum_{n=1}^{\infty} (2n+1)\,\mathrm{Im}(a_{nu} + b_{nu})\,N\,da\,d\zeta$$

$$+ \frac{2\pi^2}{T_L c k_{o_L}^3} \int_o^L \int_o^\infty \sum_{n=1}^{\infty} (2n+1)\,\mathrm{Im}(a_{nL} + b_{nL})\,N\,da\,d\zeta \tag{36}$$

$$- \frac{4\pi^2}{T_c c k_{o_o}^3} \int_o^L \int_o^\infty \sum_{n=1}^{\infty} (2n+1)\,\mathrm{Im}(a_{nc} + b_{nc})\,N\,da\,d\zeta$$

Using k = w/c and w = 2π/T and reducing

$$\varphi_{dR} = \frac{c^2}{4\pi} \int_o^L \int_o^\infty \sum_{n=1}^{\infty} (2n+1) \times \mathrm{Im} \left[(a_{nu} T_u^2 + a_{nL} T_L^2 - 2a_{nc} T_c^2) + (b_{nu} T_u^2 + b_{nL} T_L^2 - 2b_{nc} T_c^2) \right] \times N(z,a)\, da\, d\zeta \tag{37}$$

The coefficients a_n, b_n for the frequencies that are of interest here have not been tabulated. A good approximation can be made, however, if the a_n's and b_n's are expanded in a Taylor series about the center frequency f_c

$$a_n(f) = a_n(f_c) + \left. \frac{da_n}{df} \right|_{f=f_c} (f - f_c) + \frac{1}{2} \left. \frac{d^2 a_n}{df^2} \right|_{f=f_c} (f - f_c)^2 + \ldots$$

$$b_n(f) = b_n(f_c) + \left. \frac{db_n}{df} \right|_{f=f_c} (f - f_c) + \frac{1}{2} \left. \frac{d^2 b_n}{df^2} \right|_{f=f_c} (f - f_c)^2 + \ldots$$

Substituting the first two terms of these expansions into equation (37) gives:

$$\varphi_{dR} = \frac{c^2}{4\pi} \int_o^L \int_o^\infty \sum_{n=1}^{\infty} (2n+1) \times \left\{ (T_u^2 + T_L^2 - 2T_c^2)(a_{n_i} + b_{n_i}) + \left(\frac{da_{ni}}{df} + \frac{db_{ni}}{df} \right) \left[(f_u - f_c) T_u^2 + (f_L - f_c) T_L^2 \right] \right\} \times N(z,a)\, da\, d\zeta \tag{38}$$

where

$$a_{ni} = \mathrm{Im}\, a_{nc}, \quad b_{ni} = \mathrm{Im}\, b_{nc}$$

Rewriting equation (38) by noticing that only the coefficients a_n, b_n are frequency-dependent gives:

$$\varphi_{dR} = \frac{c^2}{4\pi} \int_0^L \int_0^\infty \sum (2n+1)(a_{ni} + b_{ni})(T_u^2 + T_L^2 - 2T_c^2)$$

$$\times N(Z, a)\, da\, d\zeta$$

$$+ \frac{\partial}{\partial f} \int_0^L \int_0^\infty \sum (2n+1)(a_{ni} + b_{ni}) \left[(f_u - f_c) T_u^2 + (f_L - f_c) T_L^2\right] \qquad (39)$$

$$\times N(z, a)\, da\, d\zeta$$

Some idea of the magnitude of ζdr as a function of rain rate can be found from the results in a paper by Setzer[2] in which a numerical solution is carried out for expressions of the form:

$$\varphi = \frac{c^2}{4\pi} \int_0^L \int_0^\infty T_k^2 \sum_{n=1}^{N} (2n+1)(a_{ni} + b_{ni}) N(z, a)\, da\, d\zeta$$

where T_K = period. (40)

By fixing the rain rate and varying the frequency, Setzer's data show that the second term of equation (39) is much less than the first. The sole difference between equations (39) and (40) is in the multiplicative constants T_k^2 and $(T_u^2 + T_L^2 - 2T_C^2)$. Thus given the above approximations, Setzer's data can be used to compute φdr of equation (39).

For the 20 GHz carrier with ±720 MHz sidebands,

$$(T_u^2 + T_L^2 - 2T_c^2) = 19.52 \times 10^{-24}\ \text{sec}^2$$

Setzer compiles data for

$$T_k^2 \approx 2.92 \times 10^{-21}\ \text{sec}^2$$

From Setzer

$$T_k^2\, X = \varphi^{(RR)}$$

but

$$(T_u^2 + T_L^2 - 2T_c^2)\, X = \varphi_{dR}^{(RR)}$$

so

$$\varphi_{dR}\,(RR) = \frac{(T_u^2 + T_L^2 - 2T_c^2)}{T_c^2}\quad \varphi(RR)$$

$$\varphi_{dR}\,(RR) = 0.0067\,\varphi(RR) \tag{41}$$

where: RR = Rain rate

$$X = \frac{c^2}{4\pi} \int_o^L \int_o^\infty \sum (2n+1)\,(a_{ni} + b_{ni})\, N(z, a)\, da\, dg$$

φ (RR) = Phase change in deg/km

tabulated by Setzer as a function of rain rate.

For the 30 GHz carrier with ±720 MHz sidebands, a similar procedure gives:

$$\varphi_{dR}(RR) = 0.0035\,\varphi(RR) \tag{42}$$

Table 4 lists the values found from equations (41) and (42) for various rain rates.

Table 4

Rain Rate Values

Rain Rate (mm/hr)	φ_{dR} deg/km	
	f_c = 20 GHz	f_c = 30 GHz
.25	0	0
1.25	.0147	.0124
2.5	.044	.025
5.0	.074	.017
12.5	.148	.0996
25.0	.253	.175
50.0	.431	.262
100.0	.772	.45
150.0	1.1	.612

It appears that even for extremely large rain rates over a large distance, (say 4 km), the total differential phase shifts predicted are:

$$\varphi_{dR}(f_c = 20\ \text{GHz}, RR = 150\ \text{mm/hr}) \approx 4.4^\circ$$

$$\varphi_{dR}(f_c = 30\ \text{GHz}, RR = 150\ \text{mm/hr}) \approx 2.5^\circ$$

The values in Table 4 should in no sense be presumed accurate. Within the accuracies of the model, however, a few conclusions might be drawn:

- The values of the measured differential phase are expected to be small.
- $\varphi_{dr}(f_c = 20\ \text{GHz}) > \varphi_{dr}(f_c = 30\ \text{GHz})$ for all rain rates of interest.

- If the actual differential phase is in general agreement with that predicted then almost all relevant information will be lost since the system is not expected to be sensitive to changes in phase on the order of a degree or less.

Some differential phase data have been obtained at Rosman, N.C. on day 270, 1974 during a fairly intense storm. The data have been obtained from Reference 4 and are displayed in Figure 9. Unfortunately, the data seem inconclusive since, over the relevant portions of time, the phase varies within approximately ±4° of a constant value and presumably within the errors of the system. The strong phase fluctuations near 2324 and 2328 should probably be discounted as the receiver was just losing and regaining phase lock at these times.

DISCUSSION

If a few changes are made in the data analysis procedure, the rain rates predicted from the 3.0 and 8.75 GHz radars should be in better agreement. As a basis for absolute comparison between predicted and measured rain rates, the calibration procedure may be helpful as could the measured and theoretical relations of ground-to-elevated rain rates.

Several other changes in the data analysis might be helpful:

- Range bins 4, 13, 14, 15 for the 3 GHz radar are in error by about 9.5 db. For these points, and points such that the 8.75 GHz data exists and not the 3.0 GHz data, the later can be reconstructed by use of the equations in Appendix A. The estimate of dbZ_3 at the m + 1 range bin is:

$$dbZ_3(m+1) = dbZ_8\ (m+1) - dbZ_8(m) + dbZ_3(m) + K \times .2$$

where k X .2 is the attenuation suffered by the 8.75 GHz radar between range bins m and m + 1. Normally this last term is negligible.

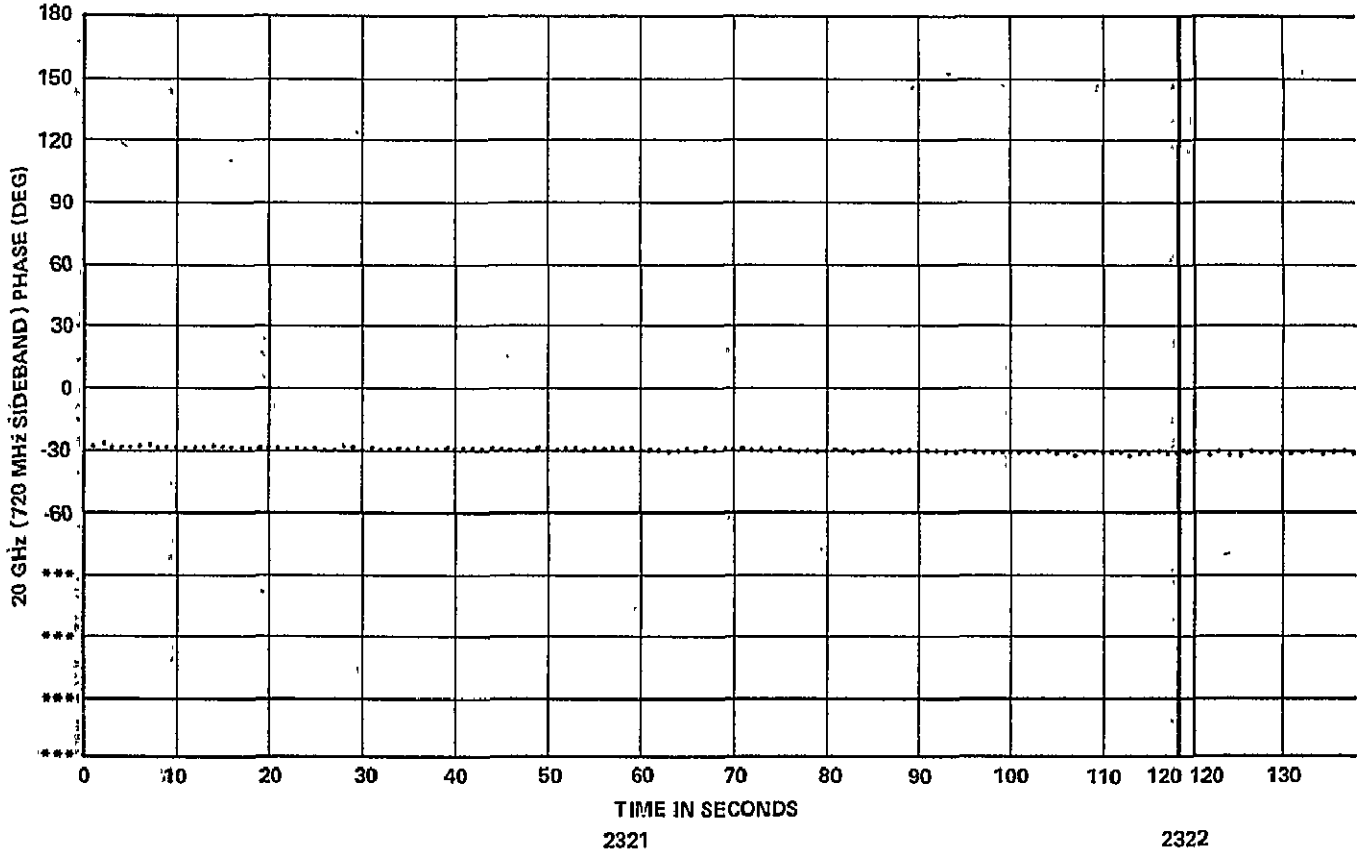

START TIME		STOP TIME
OUTER INTERVAL		
YEAR = 1974		YEAR = 1974
DAY = 270		DAY = 271
GMT = 2315		GMT = 20
INNER INTERVAL		
DAY = 270		DAY = 271
GMT = 2320		GMT = 2349

	20 GHZ	30 GHZ
TEST MODE	MT	MT
PARAMP	OFF	OFF
S/C ANT. GAIN	HI	HI
MULT. CHAIN	A	A

Figure 9. 720 MHz Sideband Phase vs Time

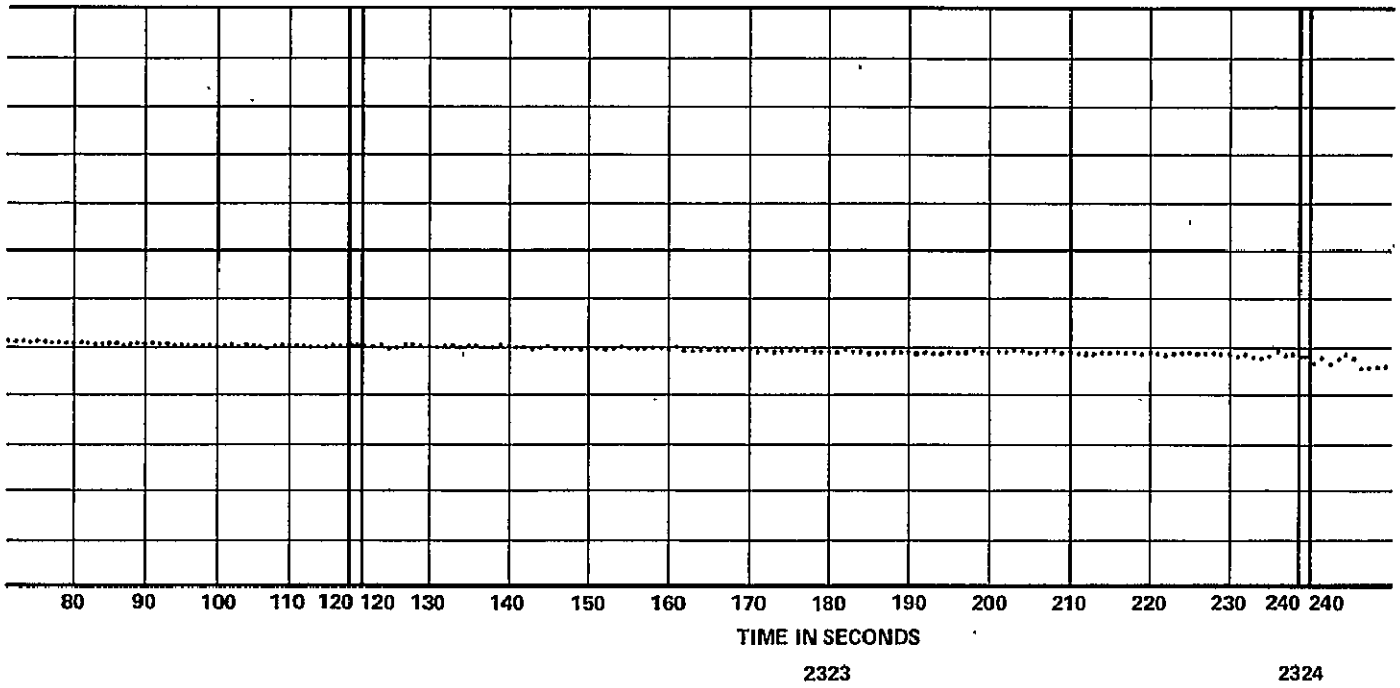

START TIME		STOP TIME	
OUTER INTERVAL			
YEAR	= 1974	YEAR	= 1974
DAY	= 270	DAY	= 271
GMT	= 2315	GMT	= 20
INNER INTERVAL			
DAY	= 270	DAY	= 270
GMT	= 2320	GMT	= 2349

	20 GHZ	30 GHZ
TEST MODE	MT	MT
PARAMP	OFF	OFF
S/C ANT. GAIN	HI	HI
MULT. CHAIN	A	A

Figure 9. 720 MHz Sideband Phase vs Time (Continued)

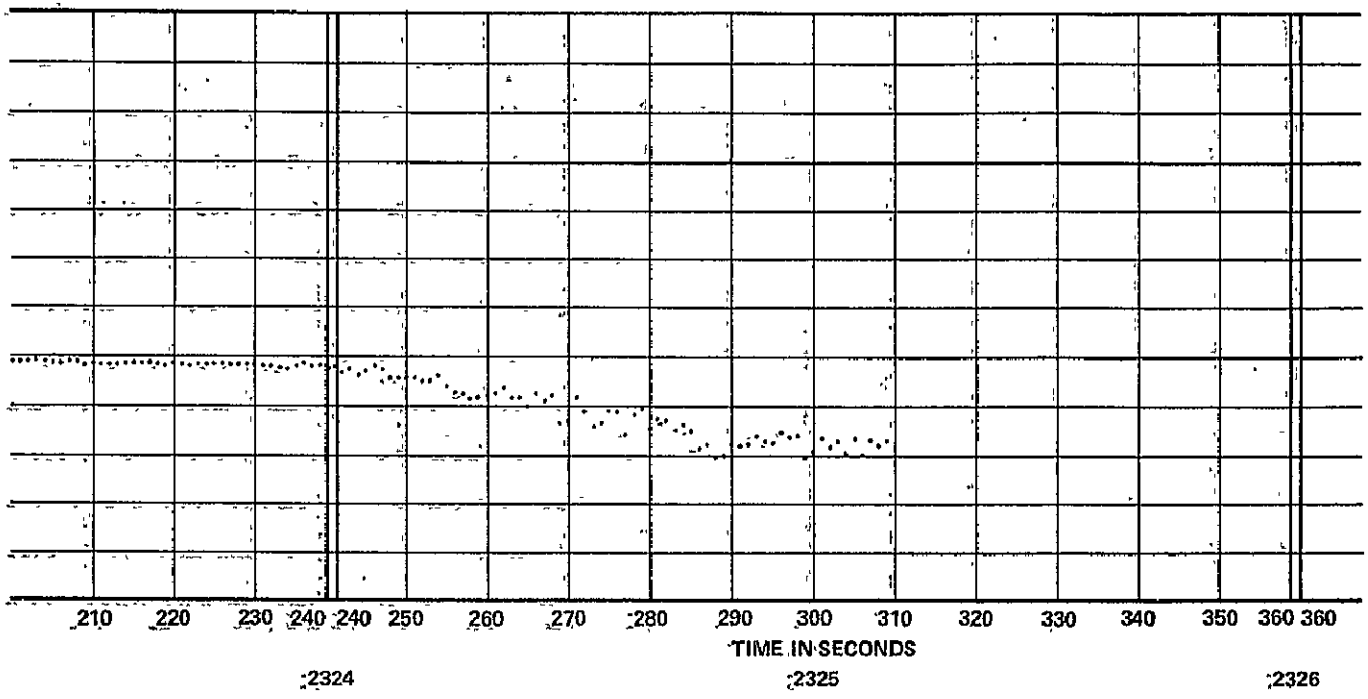

START TIME		STOP TIME	
OUTER INTERVAL			
YEAR	= 1974	YEAR	= 1974
DAY	= 270	DAY	= 271
GMT	= 2315	GMT	= 20
INNER INTERVAL			
DAY	= 270	DAY	= 270
GMT	= 2320	GMT	= 2349

	20 GHZ	30 GHZ
TEST MODE	MT	MT
PARAMP	OFF	OFF
S/C ANT. GAIN	HI	HI
MULT. CHAIN	A	A

Figure 9. 720 MHz Sideband Phase vs Time (Continued)

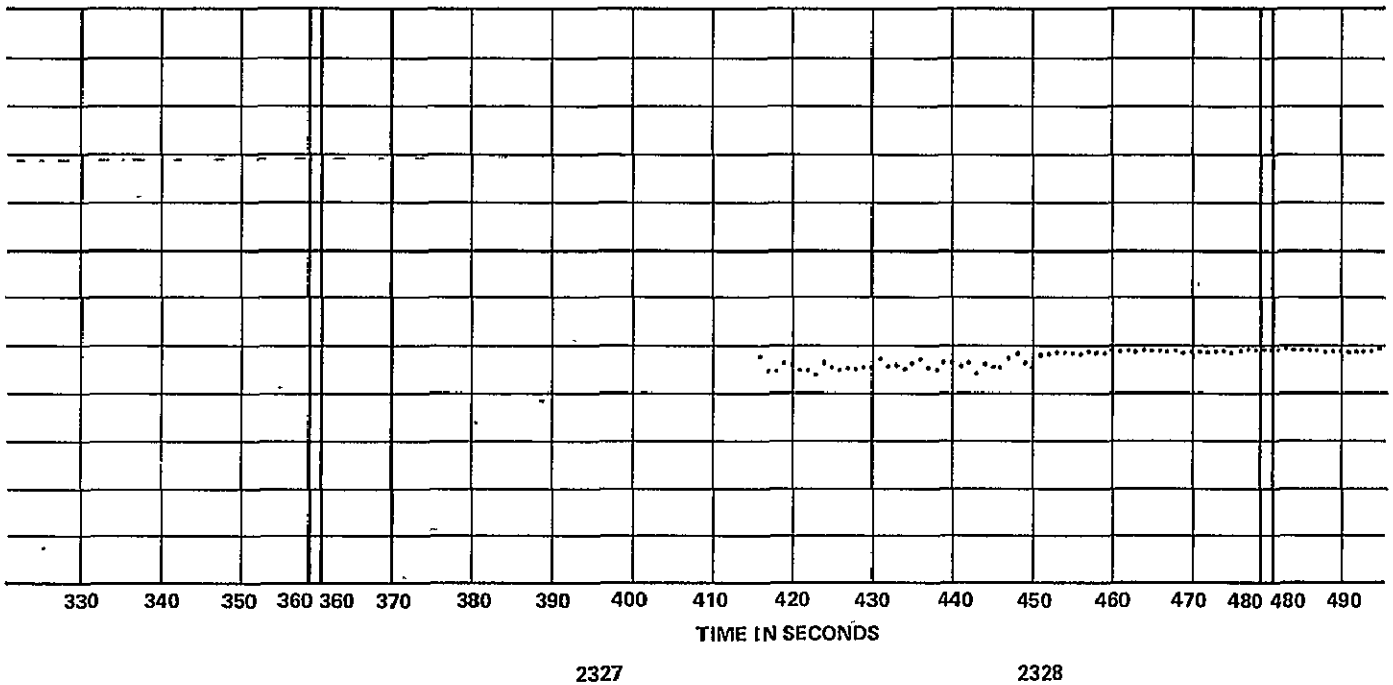

START TIME		STOP TIME	
OUTER INTERVAL			
YEAR	= 1974	YEAR	= 1974
DAY	= 270	DAY	= 271
GMT	= 2315	GMT	= 20
INNER INTERVAL			
DAY	= 270	DAY	= 270
GMT	= 2320	GMT	= 2349

	20 GHZ	30 GHZ
TEST MODE	MT	MT
PARAMP	OFF	OFF
S/C ANT. GAIN	HI	HI
MULT. CHAIN	A	A

Figure 9. 720 MHz Sideband Phase vs Time (Continued)

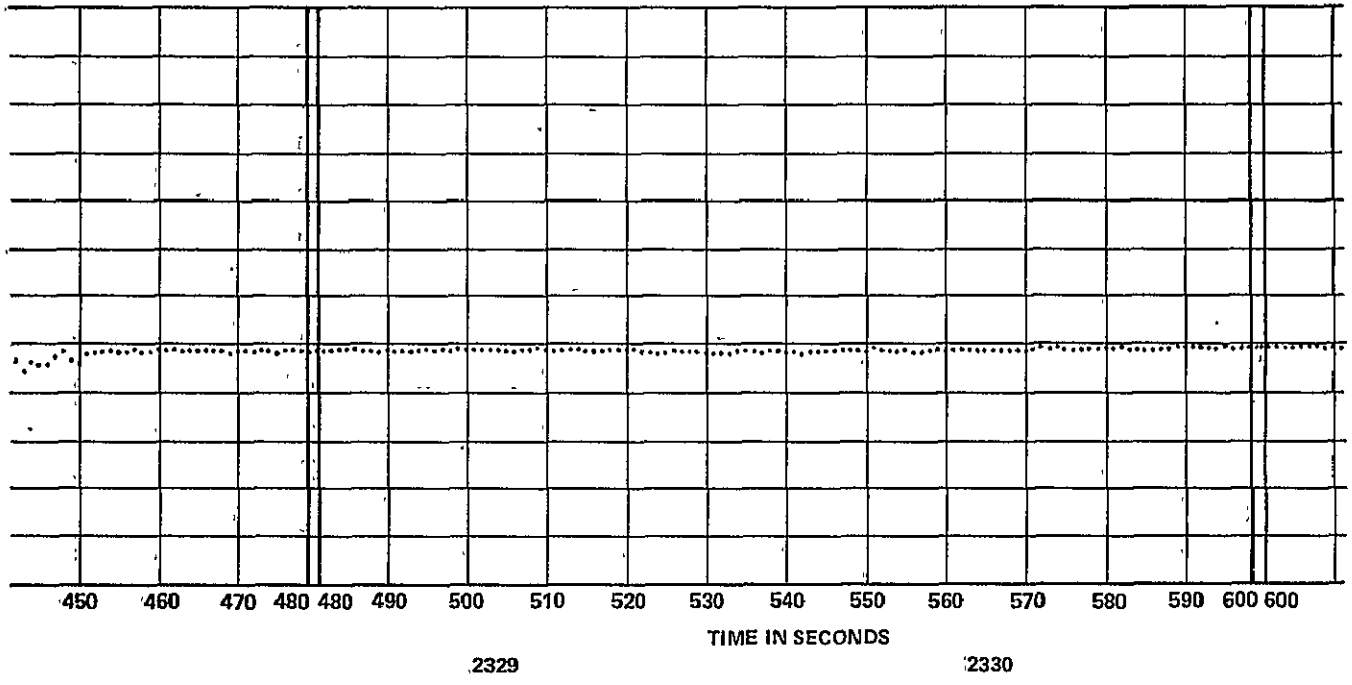

START TIME		STOP TIME	
OUTER INTERVAL			
YEAR	= 1974	YEAR	= 1974
DAY	= 270	DAY	= 271
GMT	= 2315	GMT	= 20
INNER INTERVAL			
DAY	= 270	DAY	= 270
GMT	= 2320	GMT	= 2349

	20 GHZ	30 GHZ
TEST MODE	MT	MT
PARAMP	OFF	OFF
S/C ANT. GAIN	HI	HI
MULT. CHAIN	A	A

Figure 9. 720 MHz Sideband Phase vs Time (Continued)

- The radars cannot measure rain rates of distances less than 300 m from the receiver. Nevertheless, an account should be made of the first 300 m either by rain bucket readings or by an extrapolation from the first dbZ bin. Some idea of errors introduced if these points are neglected are

$\alpha_{30} \sim 1.7$ db R = 30 mm/hr

$\alpha_{30} \sim 2.25$ db R = 40 mm/hr

$\alpha_{20} \sim .87$ db R = 30 mm/hr

$\alpha_{20} \sim 1.2$ db R = 40 mm/hr

- For those bins (at a given time) with no radar data, which occur between bins with data, lower and upper bounds for rain rates in these intervals can be assigned. Evidently, the lower bound is zero while the upper bound is the rain rate which corresponds to the minimum detectable reflectivity at that range. Thus, in the prediction of 20 and 30 GHz downlink attenuations, upper and lower bound predictions would occur. Note that in most instances the predictions will not differ by much more than 1 db.

- Due to the rain drop's deviation from sphericity, there is an added effective attenuation of the downlinks not accounted for by the radars. To correct for this effect, this attenuation due to depolarization must be added to the radar predicted attenuations. The difference, however, is slight.

- Although drop size distribution measurements do not at this time seem possible using the Goldhirsh-Katz or similar techniques, the alternative method Two Frequency Radar Technique seems to provide a fairly simple means of determining the average attenuation of the higher frequency radar.

- In the millimeter wave literature, no account has been found which describes the effects of scatterers in the vicinity of the receiver. It would be of interest to determine experimentally whether a positive correlation exists between high intensity rain rates in the near fields of the downlink receiver and errors between predicted and measured attenuation values.

- Error analyses of Z due to target fluctuations could be incorporated into the present computer programs. Occasional measurements of noise and clutter levels are necessary inputs to the statistical model. Such procedures would impose limits on the maximum possible accuracy of radar predictions of downlink attenuations.

REFERENCES

1. Medhurst, R. G., Rainfall Attenuation of Centimeter Waves: Comparison of Theory and Measurement, IEEE Transactions on Antennas and Propagation, 13, No. 4, July 1965, pp. 550-563.

2. Setzer, D. E., Computed Transmission Through Rain at Microwave and Visible Frequencies, Bell System Tech. J., 49, No. 8, Oct. 1970, pp. 1873-1892.

3. ATS-6 Millimeter Wave Propagation Experiment. Contract No. NAS 5-20797, Feb. 1975, Prepared by Westinghouse.

4. Stephens, J. J., Radar Cross Sections for Water and Ice Spheres, J. Met., vol 18, June 1961, pp. 348-359.

5. Battan, L. I., Radar Observation of the Atmosphere, Chicago: Univ. of Chicago Press, 1973, pp. 42, 73, 95.

6. Ippolito, L. J., 20 and 30 gHz Millimeter Wave Experiments with the ATS-6 Satellite, NASA X-951-75-211, August 1975

7. Personal Communication with L. Ippolito.

8. Fang, D. J., Harris, J. M., Hyde, G., Measurement of ATS-6 20/30 GHz Signals at Clarksburg, Maryland, Presented at 1975 URSI meeting.

9. Foote, G. B., and du Toit, P. S., Terminal Velocity of Rain Drops Aloft, Journal of Applied Meteorology, vol 8, April 1969, pp. 249-253.

10. Goldhirsh, J., Katz, I., Estimation of Raindrop Size Distribution Using Multiple Wavelength Radar Systems, Radio Science, Vol. 9, No. 4, April 1974, pp. 439-446.

11. Katz, I., Goldhirsh, J. Estimation of the Rain Drop Distribution Using an S-Band Radar and a Rain Gauge. Memo. MPD 73U-063, 10 August 1973.

12. Goldhirsh, J., Katz, I., Dual Wavelength Technique to Establish Raindrop Size Distribution. Memo. MPD 73U-039, 10 May 1973.

13. Stagryn, A., Error Analysis of the Goldhirsh-Katz Method of Rainfall Rate Determination by the use of a Two Frequency Radar, Aerojet Electrosystems Co., Report 1833TR-4, Jan., 1975.

14. Marshall, J. S., Hitschfeld, W., Interpretation of the Fluctuating Echo from Randomly Distributed Scatters. Part I. Canadian J. Physics 31:962-94, 1953.

15. van de Hulst, H. C., Light Scattering by Small Particles, New York: John Wiley Sons, Inc., 1957.

APPENDIX A

Z-R RELATIONS

$$Z_{3.0} = \sum_i N_{D_i} D_i^6 \delta_{3_i} \quad \vec{\lim} \int N(D)\, D^6 \delta_3(D) dD \quad mm^6/m^3$$

$$Z_{8.75} = \sum N_{D_i} D_i^6 \delta_{8_i} \quad \vec{\lim} \int N(D)\, D^6 \delta_8(D)\, dD \quad mm^6/m^3$$

where

$$\delta = \frac{\sigma_{mie}}{\sigma_{rayl}}$$

is the ratio of the backscattering cross-sections as predicted by the Mie and Rayleigh theories. Note that δ is a function not only of λ and D but also of temperature. The calculations use a rain temperature of 18°C. The values of δ_{3_i}, δ_{8_i} are taken from Reference 3 of the main report. Velocity vs. diameter and rain rate vs diameter are taken from Reference 2.

The expression for N_o is given in Reference 1 of the main report.

$$N_D(m^{-3}) = \frac{RR \times (\% \text{ tot vol})}{1.885\, \nu D^3}$$

in which

RR = mm/hr
ν = m/sec
D = cm

Computing $Z_{3.0}$ and $Z_{8.75}$ for various rain rates and fitting this data to an aR^b form by a least squares fit then

$$Z_{3.0} = 315.5\ R^{1.457}$$

$$Z_{8.75} = 307.1\ R^{1.546}$$

If b is fixed to 1.5 then the best fit becomes:

$$Z_{3.0} = 261.16\ R^{1.5}$$

$$Z_{8.75} = 341.715\ R^{1.5}$$

These values should be compared to those given in Reference 5 of the main report.

Marshall - Palmer (0°C)

$$Z_{9.345} = 275\ R^{1.55}$$

$$Z_{3.0} = 210\ R^{1.6}$$

Gunn & East (18°C)

$$Z_{9.345} = 310\ R^{1.56}$$

$$Z_{3.0} = 210\ R^{1.6}$$

Mueller & Jones (0°C)

$$Z_{9.345} = 890\ R$$

$$Z_{3.0} = 810\ R$$

APPENDIX B

K - Z RELATIONS

Δk (db/km) can be found directly from Medhurst's data. A mean square fit is then performed:

$$\Delta k \text{ (db/km)} = .006569\, R^{1.29}$$

$$\Delta k \text{ (db/km)} = 3.99 \times 10^{-5}\, Z_{3.0}^{0.88}$$

$$\Delta k \text{ (db/km)} = 5.5444 \times 10^{-5}\, Z_{8.75}^{0.83}$$

where

$$\Delta k \text{ (db/km)} = \text{att } (Z_{8.75})_{db} - \text{att } (Z_{3.0})_{db} \approx \text{att } (Z_{8.75})_{db}$$

The plots:

Δk vs R

Δk vs $Z_{3.0}$

$Z_{8.75}$ vs R

$Z_{3.0}$ vs R

are given on the following pages.

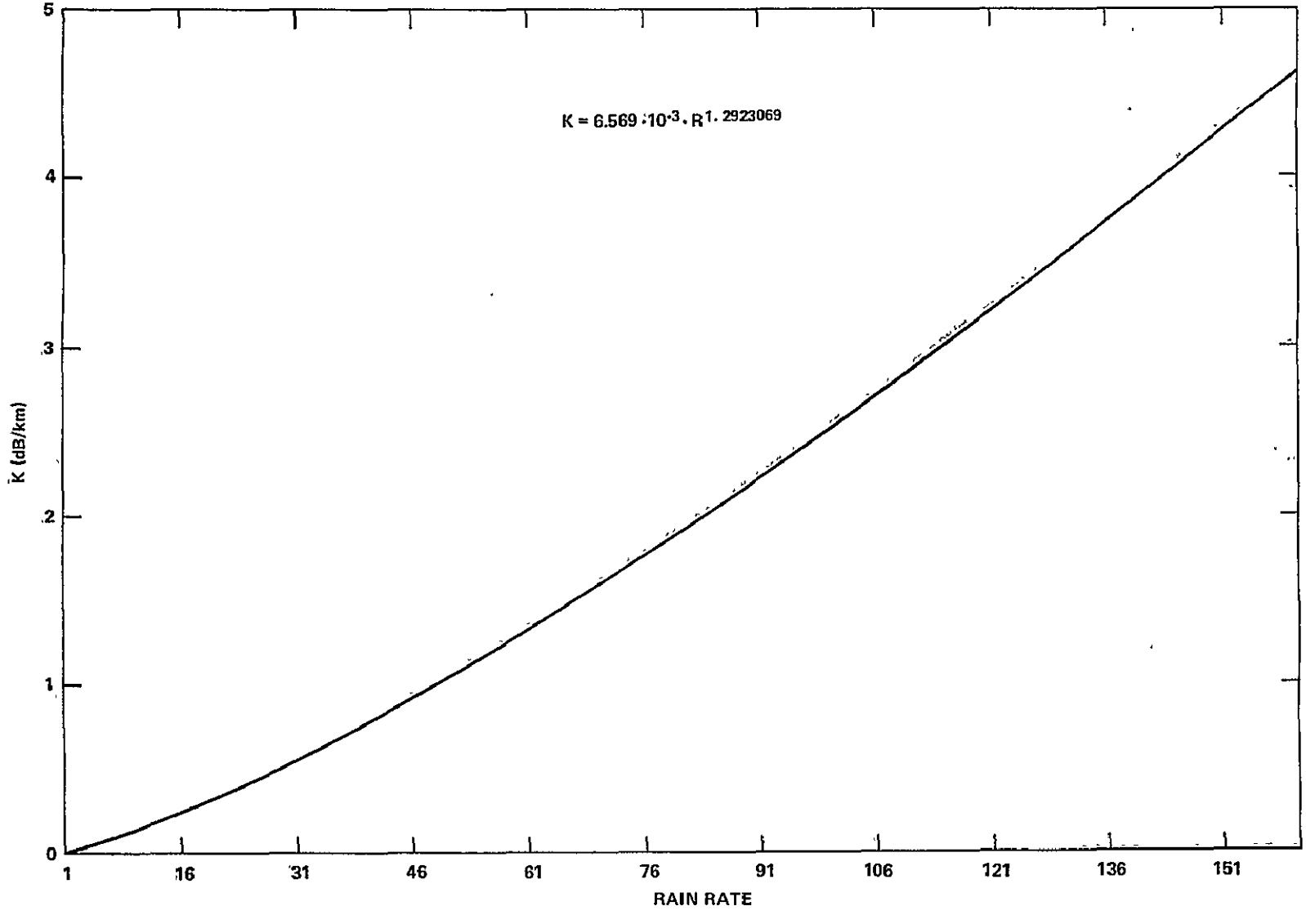
K = 6.569 ·10·3 · R1. 2923069
K (dB/km)
RAIN RATE
0
1
2
3
4
5
1
16
31
46
61
76
91
106
121
136
151

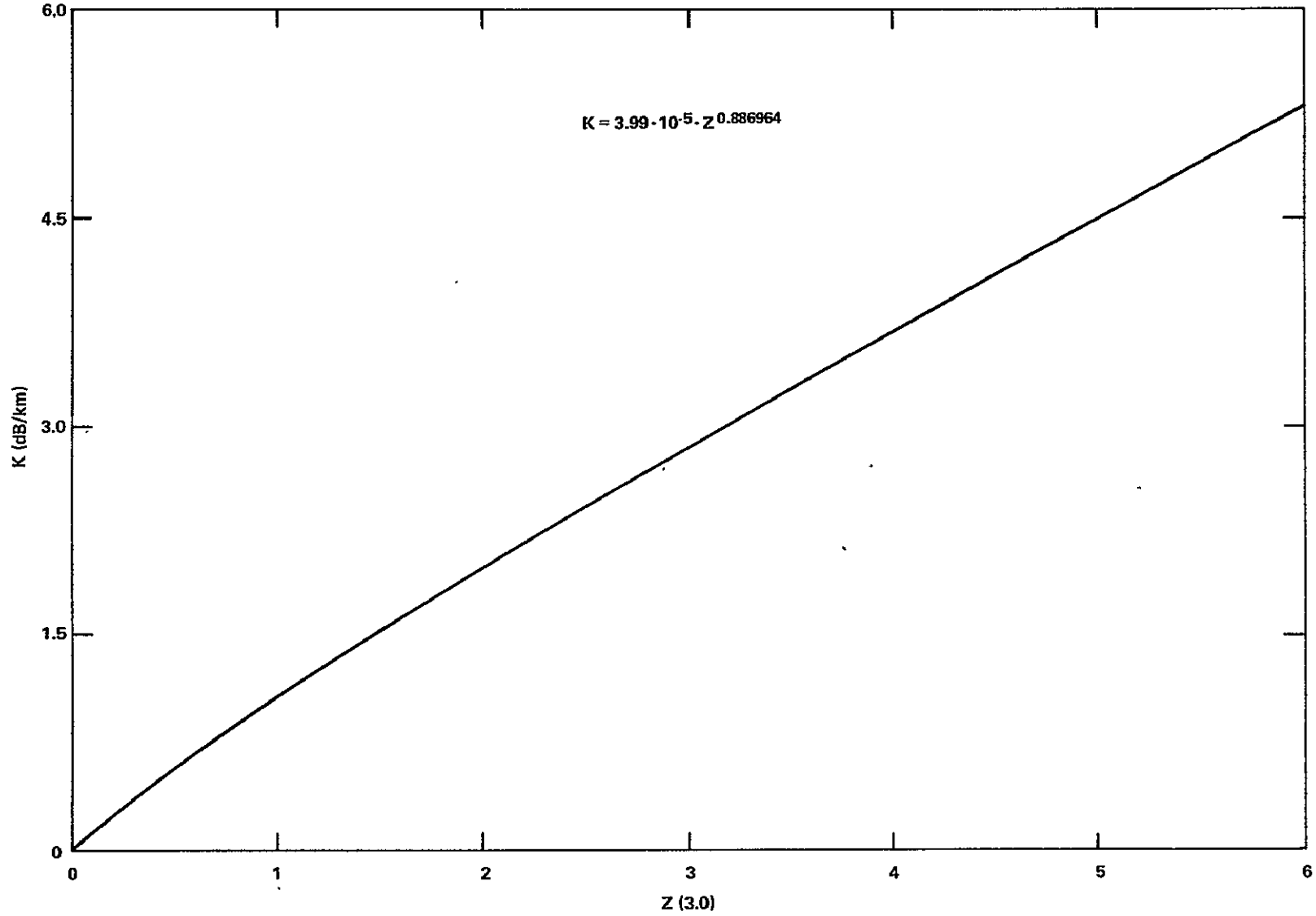
K = 3.99·10⁻⁵·Z^0.886964
K (dB/km)
Z (3.0)
6.0
4.5
3.0
1.5
0
0
1
2
3
4
5
6

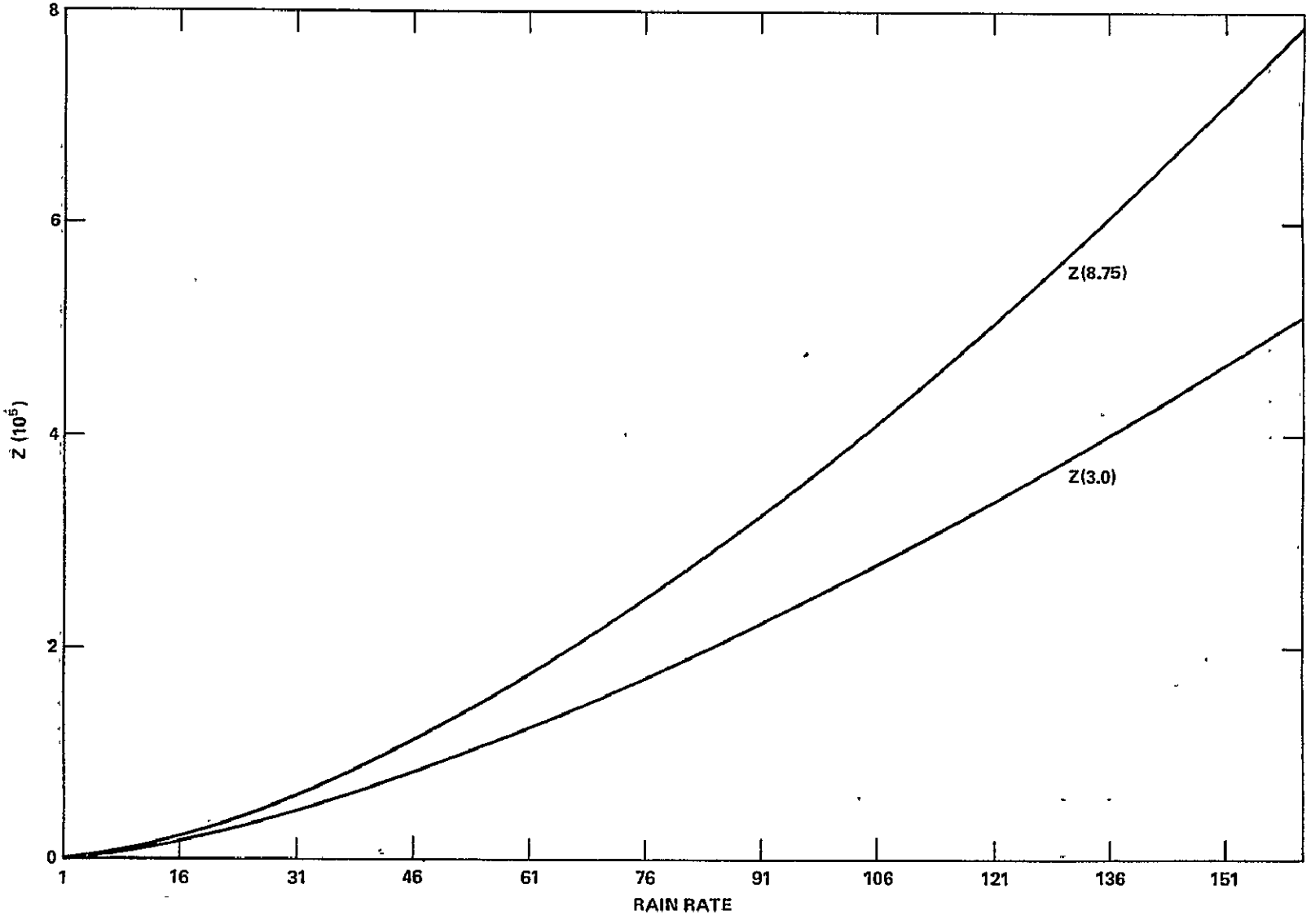
8
6
4
2
0
Z (10⁵)
Z(8.75)
Z(3.0)
1
16
31
46
61
76
91
106
121
136
151
RAIN RATE